INORGANIC CHEMISTRY
FRONTIERS

RESEARCH ARTICLE

View Article Online
View Journal | View Issue



Cite this: *Inorg. Chem. Front.*, 2024, **11**, 1070

# Exploring the use of rigid 18-membered macrocycles with amide pendant arms for Pb(II)-based radiopharmaceuticals†

Charlene Harriswangler, [a] Brooke L. McNeil,[b,c] Isabel Brandariz-Lendoiro,[a] Fátima Lucio-Martínez,[a] Laura Valencia, [d] David Esteban-Gómez, [a] Caterina F. Ramogida *[b,c] and Carlos Platas-Iglesias *[a]

We report a detailed investigation on the use of chelators PYTAM, $H_4$PYTAMGly, *CHX*-PYTAM and $H_4$*CHX*-PYTAMGly for the complexation of Pb(II)-radioisotopes with potential use in the preparation of radiopharmaceuticals. The macrocyclic backbones from which the chelators are prepared, PYAN (3,6,10,13-tetraaza-1,8(2,6)-dipyridinacyclotetradecaphane) or *CHX*-PYAN ((4$^1$*R*,4$^2$*R*,10$^1$*R*,10$^2$*R*)-3,5,9,11-tetraaza-1,7(2,6)-dipyridina-4,10(1,2)-dicyclohexanacyclododecaphane), are readily synthesized in high yields using a Ba(II) template synthesis. The single difference between the two backbones is that while PYAN contains ethylene spacers, *CHX*-PYAN incorporates more rigid cyclohexyl spacers. The pendant arms incorporated into the backbone were strategically chosen, selecting amide pendants of different nature, compatible with the borderline Lewis acid character of Pb(II). To study the complexation of Pb(II), first, a detailed characterization of the non-radioactive complexes was carried out, including X-ray crystallography, NMR, and the determination of chelator protonation and stability constants of the complexes. Once the complexes were fully characterized and showed favourable properties towards Pb(II), a radiochemical study using the SPECT compatible radioisotope lead-203 was performed. Although all tested chelators sufficiently complexed lead-203 and presented excellent complex stability in human serum, it was found that novel chelator CHX-PYTAM was superior over the others due to its high kinetic inertness. This effect is due to increased rigidity of the complex with cyclohexyl spacers in the backbone and use of primary amides, over secondary amides, as pendant arms and thus this chelator is a promising candidate for future *in vivo* studies.

Received 14th November 2023,
Accepted 21st December 2023

DOI: 10.1039/d3qi02354k

rsc.li/frontiers-inorganic



## Introduction

There are a wide variety of radioactive metals that have potential use in radiopharmaceutical compounds, both for diagnostic and therapeutic applications.[1] Within the family of diagnostic isotopes we can find positron ($\beta^+$) emitters that can be used for positron emission tomography (PET) imaging, such as commonly used gallium-68 ($^{68}$Ga, $t_{1/2}$ = 67.7 min), or isotopes that directly emit gamma (γ-) rays for SPECT (single photon emission computed tomography) imaging, such as technetium-99m ($^{99m}$Tc, $t_{1/2}$ = 6.00 h).[2] Therapeutic isotopes, on the other hand, release cytotoxic radiation and can be divided into three categories depending on the type of radiation that is produced: alpha (α)-emitters, beta ($\beta^-$)-emitters and Auger electron emitters.[3]

Nowadays, the emerging field of theranostics combines both applications of radioisotopes in order to achieve a more personalized treatment.[4] First, a diagnostic agent is administered to evaluate the uptake of the radiopharmaceutical and if the uptake is high, the therapeutic is administered subsequently. There are different combinations of isotopes that can be used in this procedure, "true theranostics", same-element isotope pairs, and different-element pairs.[5,6] True theranostic radionuclides emit both imaging compatible radiation and therapeutic particles, such as the $\beta^-$-emitter lute-

[a]*Universidade da Coruña, Centro Interdisciplinar de Química e Bioloxía (CICA) and Departamento de Química, Facultade de Ciencias, 15071 A Coruña, Galicia, Spain. E-mail: carlos.platas.iglesias@udc.es*
[b]*Department of Chemistry, Simon Fraser University, Burnaby, BC, Canada. E-mail: caterina_ramogida@sfu.ca*
[c]*Life Sciences Division, TRIUMF, Vancouver, BC, Canada*
[d]*Departamento de Química Inorgánica, Facultad de Ciencias, Universidade de Vigo, As Lagoas, Marcosende, 36310 Pontevedra, Spain*

†Electronic supplementary information (ESI) available: $^1$H, $^{13}$C, high-resolution crystal data and structure refinement details, thermodynamic constant determination and radiolabeling experiments. CCDC 2305213 and 2305214. For ESI and crystallographic data in CIF or other electronic format see DOI: **https://doi.org/10.1039/d3qi02354k**

tium-177 ($^{177}$Lu, $t_{1/2}$ = 6.64 days) which emits an accompanying γ-ray compatible with SPECT imaging. Although a true theranostic may be convenient, one of the drawbacks of the use of these isotopes, is the potential for off target effects if there is not significant uptake shown in the image.[7] This is why, when evaluating the use of $^{177}$Lu for patient treatment, $^{68}$Ga is often used for pre-therapy imaging and uptake evaluation.[8] However, when using a different-element pair, the pharmacokinetics of both radiopharmaceuticals may not be identical, which could be problematic if the update of the imaging tracer does not accurately reflect the biodistribution of the therapeutic pharmaceutical.[5] This can be avoided by using a same element isotope pair, where two different isotopes of the same element are appropriate for either diagnosis or therapy, such as the lead-212 ($^{212}$Pb, $t_{1/2}$ = 10.6 h)/lead-203 ($^{203}$Pb, $t_{1/2}$ = 51.9 h) theranostic pair.[9,10]

The $^{212}$Pb/$^{203}$Pb theranostic pair has emerged in recent years as a promising candidate for use in personalized theranostics, which has triggered efforts focused on finding chelators that are adequate to take advantage of the potential of this pair.[10–15] The $^{203}$Pb-radionuclide emits a 279 keV (81%) γ-photon, and can be produced through proton bombardment of Tl on medical cyclotrons *via* either the $^{203}$Tl (p,n) $^{203}$Pb reaction or the $^{205}$Tl (p,3n) $^{203}$Pb reaction.[10,16] The $^{212}$Pb-radionuclide emits β$^-$-particles and, indirectly, an α-particle through the decay of its daughters bismuth-212 ($^{212}$Bi, $t_{1/2}$ = 60.6 min) or polonium-212 ($^{212}$Po, $t_{1/2}$ = 294.3 ns) and can be obtained *via* different generators based on isotopes from the thorium-228 ($^{228}$Th, $t_{1/2}$ = 1.9 years) decay series.[17] The half-life of this isotope pairs nicely with the biological half-life of small biomolecules, like peptides, that can bind to targets such as prostate-specific membrane antigen (PSMA) and somatostatin receptors (SSTRs) which are overexpressed in some tumours.[18–20] It should be noted that phase 1 clinical trial results using [$^{212}$Pb]Pb-DOTAMTATE (bifunctional chelator [DOTAM] coupled to SSTR-targeting peptide [TATE]) have recently been published, in which SSTR-expressing neuroendocrine tumours are targeted, with very promising results, showing an objective radiologic response (ORR) of 80% compared to an ORR of 13% obtained with [$^{177}$Lu]Lu-DOTATATE (bifunctional chelator [DOTA] coupled to SSTR-targeting peptide [TATE]).[20]

One of the most commonly used strategies to harness the decay properties of these metals *in vivo* is through the use of bifunctional chelators (BFCs), in which the radiometal of interest is coordinated by a chelator and attached, through a linker, to a biological targeting vector such as a peptide or an antibody.[21,22] This allows for the radioactivity to be delivered selectively to the diseased tissue, while minimally damaging surrounding healthy tissue.[23] Coordination chemistry plays a key role in the design of these BFCs, as it is necessary to tailor the properties of the chelator to the properties of each specific metal to obtain thermodynamically stable and kinetically inert complexes, to avoid the release of the metals *in vivo* and possible toxicity.[24]

When designing a new chelator, Pearson's hard–soft acid–base (HSAB) principle should be considered, so that donor atoms matching the metal ion are incorporated into the structure of the chelator.[25] Stable complexation of lead(II), a borderline acid, is generally achieved using amide donor groups, borderline bases, with the CYCLEN (1,4,7,10-tetraazacyclododecane)-based macrocyclic derivative DOTAM being the leading chelator for this metal ion (Scheme 1).[26,27] Macrocyclic chelators are often preferred as they are pre-organized in a way such that the entropic penalty associated with coordination is reduced, resulting in thermodynamically stable and kinetically inert complexes.[28–30] In recent years, the effect of incorporating rigid spacers into the backbone of different acyclic ligands has been studied, in most occasions resulting in higher kinetic inertness.[31–34] However, when studying the effect of the incorporation of a cyclohexyl spacer into the backbone of the 18-membered macrocycle $H_2$MACROPA, the kinetic lability of the resulting lanthanide complexes actually increased.[35]

Concerning the use of macrocyclic chelators for biomedical applications, DOTA (2,2′,2″,2‴-(1,4,7,10-tetraazacyclododecane-1,4,7,10-tetrayl)tetraacetic acid) is the most commonly used system.[36] This platform is based on the azamacrocycle CYCLEN, although macrocycles such as TACN (1,4,7-triazacyclononane) and CYCLAM (1,4,8,11-tetraazacyclotetradecane) have also been extensively investigated.[37] The popularity of these systems is mainly due to the presence of amine nitrogen atoms that can be used to functionalise the macrocycle with additional pendant arms to increase the denticity of the systems. Apart from these systems, larger 18-membered macrocycles incorporating ether or pyridine donors, have been studied in recent years for the complexation of large radiometals.[38–44] Although not yet reported for radiopharmaceutical uses, PYTAM (Scheme 1) is a decadentate macrocyclic chelator with four acetamide pendant arms, belonging to the PYAN family, first used for the complexation of lanthanides, resulting in very inert complexes.[45,46]

Herein, we present a study on the coordination ability towards [$^{nat/203}$Pb]Pb(II) of PYTAM and another three new decadentate hexaazamacrocylic chelators. Additional rigidity was introduced into the PYTAM framework by incorporating two cyclohexyl units, giving rise to the new chelator *CHX*-PYTAM. To improve solubility of these chelators at more basic pH values, the acetamide groups were substituted with glycinate arms giving chelators $H_4$PYTAMGly and $H_4$*CHX*-PYTAMGly. The intermediate HSAB character of the primary and secondary amides, along with the pyridyl groups present in the structure of these chelators, is expected to pair nicely with coordination preference of Pb(II). The [$^{nat}$Pb]Pb(II) complexes were prepared *in situ* and studied in solution through a combination of multinuclear ($^1$H, $^{13}$C, $^{207}$Pb) NMR spectroscopy and DFT calculations. We also report the X-ray crystal structures of two of the complexes. Protonation constants of two of the chelators and the stability constants of the resulting Pb(II) complexes were determined through a combined spectrophotometric and potentiometric approach. Subsequently, radiolabelling and stability studies were performed with [$^{203}$Pb]Pb(II) produced using a 13 MeV cyclotron. It should be noted that asymmetric functionalization of 3,6,10,13-tetraaza-1,8(2,6)-dipyridinacyclotetradecaphane, the backbone on which the

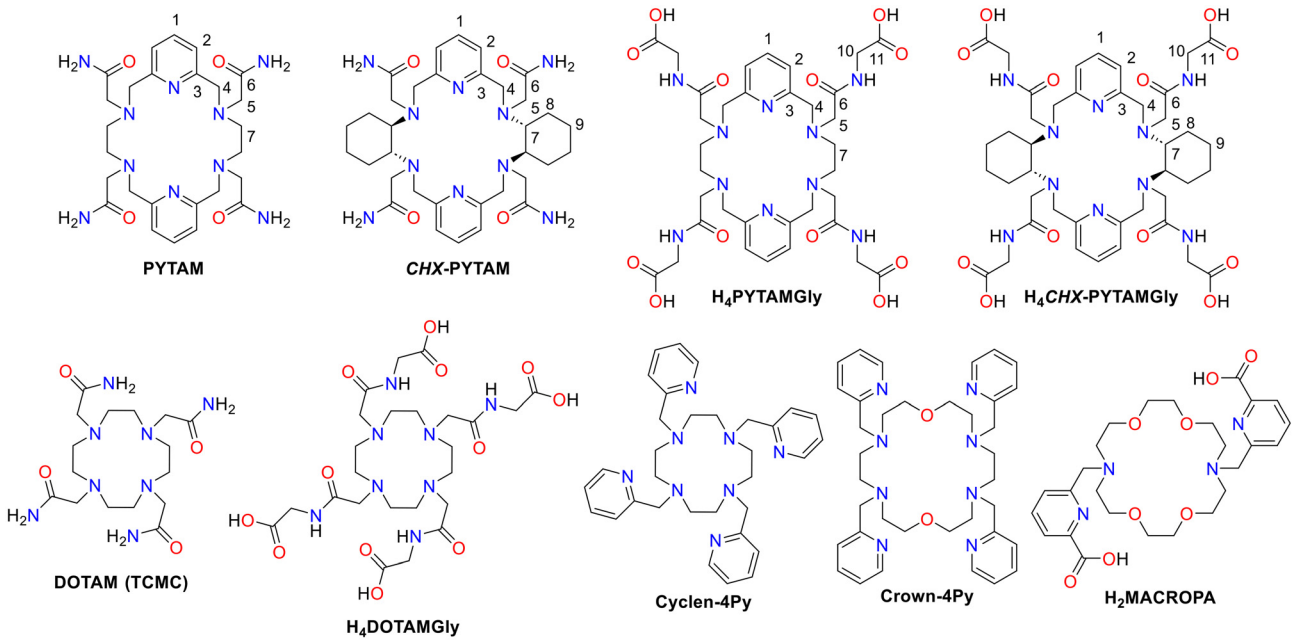


**Scheme 1** Chelators discussed in this work and numbering scheme used for NMR spectral assignment.

chelators are based, has been recently described,[42] paving the way for bifunctional systems based on this platform.

## Results and discussion

### Synthesis of the chelators

*CHX*-PYTAM was synthesized following a procedure similar to the one reported previously for PYTAM,[45] through alkylation of macrocycle *CHX*-PYAN with 2-bromoacetamide (Scheme 2), yielding *CHX*-PYTAM as a white solid (40% yield). The *CHX*-PYTAM precursor was obtained by a Ba(II)-templated Schiff-base condensation reaction, following a slight modification of the method reported by Jackels.[47] $H_4$PYTAMGly and $H_4$*CHX*-PYTAMGly were prepared through alkylation of the corresponding macrocyclic backbone with *tert*-butyl (2-chloroacetyl)glycinate followed by deprotection of the *tert*-butyl groups using TFA, affording the final chelators in 13% and 44% yields, respectively, over the two steps (see Experimental section for details).

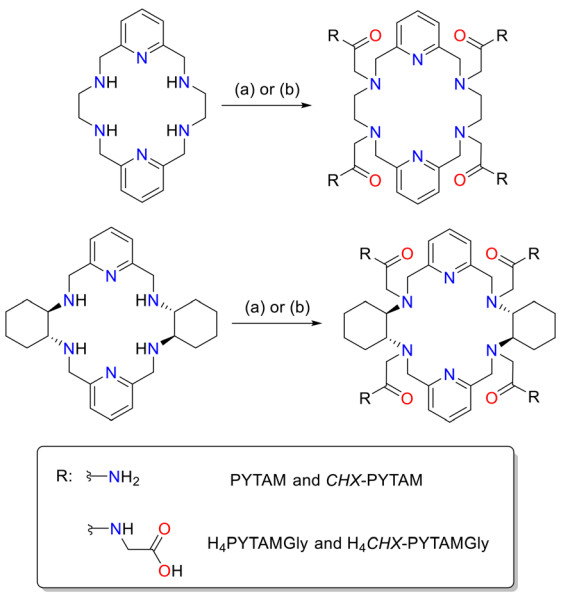


**Scheme 2** General procedure for the synthesis of the chelators. (a) Bromoacetamide and $Na_2CO_3$ in acetonitrile. (b) *tert*-butyl (2-chloroacetyl) glycinate $K_2CO_3$ in acetonitrile, followed by 1 : 1 TFA : $CH_2Cl_2$.

### X-ray crystal structures of $[Pb(PYTAM)](PF_6)_2$ and $[Pb(H_4PYTAMGly)](NO_3)_2{\cdot}5H_2O$

Addition of excess $KPF_6$ to an aqueous solution of the $[Pb(PYTAM)]^{2+}$ complex and slow evaporation of an acidic solution of the $[Pb(H_4PYTAMGly)]^{2+}$ complex provided single crystals suitable for X-ray analysis (Fig. 1 and Fig. S1, S2, ESI†). Bond distances of the Pb(II) coordination environments are listed in Table 1. Compound $\mathbf{[Pb(PYTAM)](PF_6)_2}$ crystallizes in the centrosymmetric orthorhombic *Fddd* space group, with the asymmetric unit showing only one quadrant of the molecule due to its crystallographically-imposed $D_2$ symmetry. Crystals contain two non-coordinated $PF_6^-$ anions involved in hydrogen-bonding interactions with the chelator amide N–H groups. On the other hand, $\mathbf{[Pb(H_4PYTAMGly)](NO_3)_2{\cdot}5H_2O}$ crystallizes in the monoclinic $P2_1/c$ space group and contains a network of water molecules interacting *via* hydrogen bonds with nitrate anions the protonated terminal carboxylate groups of the glycinate arms.

The Pb(II) ion in $\mathbf{[Pb(PYTAM)](PF_6)_2}$ is ten-coordinated by the chelator, which binds through the six N donor atoms of

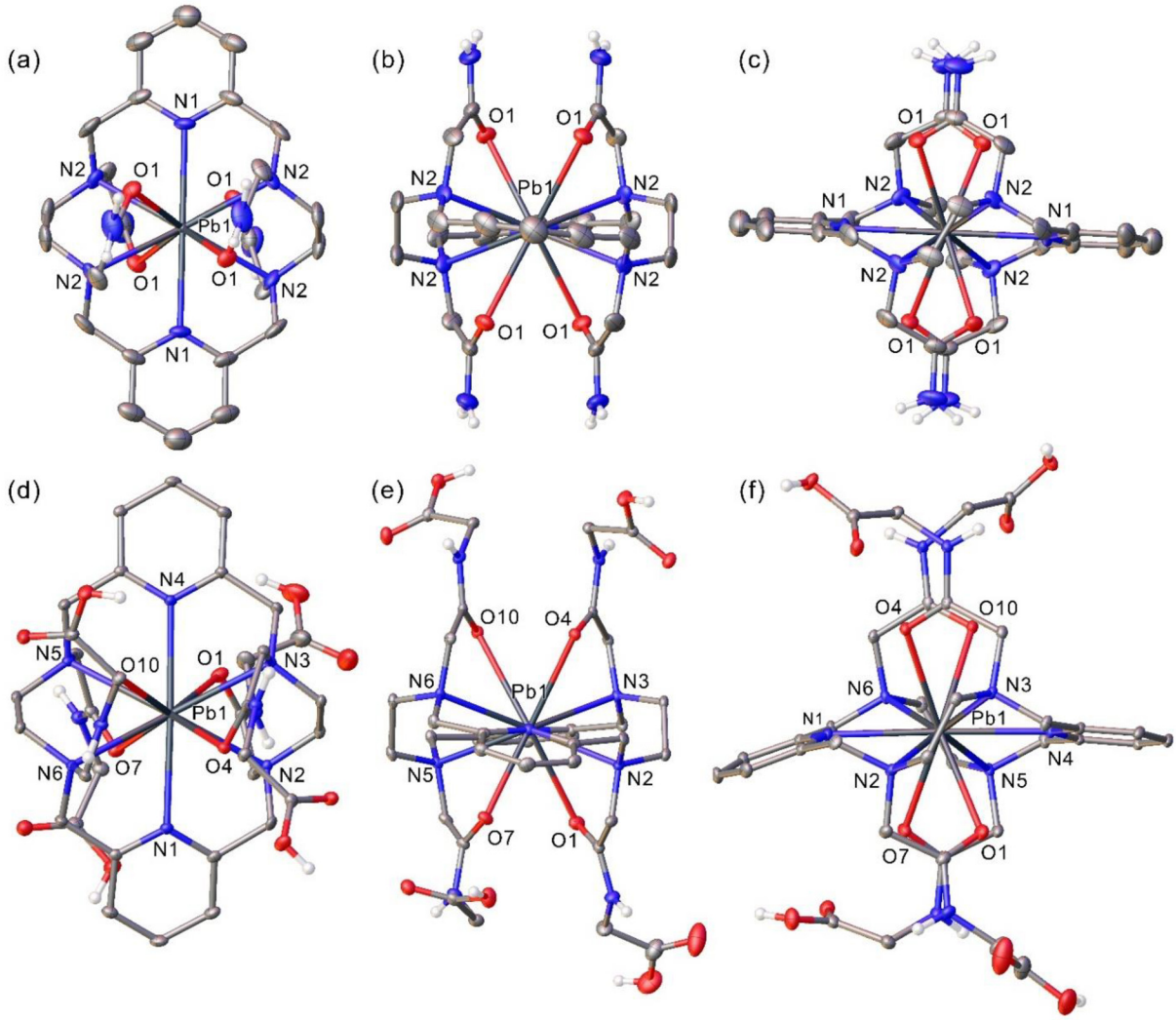


**Fig. 1** ORTEP views (30%) of the cations present in the crystal structures of **[Pb(PYTAM)](PF$_6$)$_2$** [(a)–(c)] and **[Pb(H$_4$PYTAMGly)](NO$_3$)$_2$·5H$_2$O** [(d)–(f)] with atom labelling. Hydrogen atoms bonded to C atoms, solvent molecules and anions are omitted for simplicity.

**Table 1** Interatomic distances (Å) of the metal coordination environment in crystals of **[Pb(PYTAM)](PF$_6$)$_2$** and **[Pb(H$_4$PYTAMGly)](NO$_3$)$_2$·5H$_2$O**

| **[Pb(PYTAM)](PF$_6$)$_2$** | | **[Pb(H$_4$PYTAMGly)](NO$_3$)$_2$·5H$_2$O** | |
|---|---|---|---|
| Pb(1)–N(1) | 2.646(6) | Pb(1)–N(1) | 2.650(2) |
| | | Pb(1)–N(4) | 2.623(2) |
| Pb(1)–N(2) | 2.732(5) | Pb(1)–N(2) | 2.733(2) |
| | | Pb(1)–N(3) | 2.7109(19) |
| | | Pb(1)–N(5) | 2.7663(19) |
| | | Pb(1)–N(6) | 2.753(2) |
| Pb(1)–O(1) | 2.791(4) | Pb(1)–O(1) | 2.8648(19) |
| | | Pb(1)–O(4) | 2.7828(17) |
| | | Pb(1)–O(7) | 2.6935(18) |
| | | Pb(1)–O(10) | 2.9217(17) |

the macrocycle and the four amide O atoms. The Pb–N distances involving pyridyl N atoms (2.646(6) Å) are ~0.09 Å shorter than those to amine N atoms (2.732(5) Å), a trend that is consistent with X-ray structures reported in the literature for eight-coordinate Pb(II) complexes.[15,48] The distances between the metal ion and the O donor atoms (2.791(4) Å) are longer than those involving N donor atoms, a situation observed previously for complexes containing amide groups such as $[Pb(DOTAM)]^{2+}$,[49] or even negatively charged carboxylate groups (*i.e.* $[Pb(DOTA)]^{2-}$).[50]

The Pb(II)-donor distances in $[Pb(H_4PYTAMGly)]^{2+}$ point to a slight distortion of the metal coordination environment compared to **[Pb(PYTAM)](PF$_6$)$_2$** (Table 1). Indeed, one of the Pb–O distances is particularly short [Pb(1)–O(7) = 2.6935(18) Å], while the remaining three Pb–O distances are in the range of 2.78 to 2.92 Å. Similarly, the distances to amine N atoms differ by up to ~0.06 Å. The deformation of the coordination sphere appears to be related to steric interactions involving methylene protons of neighbouring terminal acetic acid groups, which display H···H distances as short as 2.77 Å. The distortion of the metal coordination sphere is also reflected in the angle

involving the two pyridyl N atoms and the metal ion, which is linear in $[Pb(PYTAM)]^{2+}$ takes a value of 177.99(6)° in $[Pb(H_4PYTAMGly)]^{2+}$, with the pyridine rings being slightly bent towards the hemisphere of the metal coordination environment where O(7) and O(1) are situated. The slight alteration of the Pb(II) coordination sphere in $[Pb(H_4PYTAMGly)]^{2+}$ does not appear to be related to a significant activity of the $6s^2$ lone pair. In fact, previous works associated the stereochemical activity of the lone pair with a polarization of the $6s^2$ lone pair with a significant 6p contribution.[51,52] However, the analysis of the natural bond orbitals using DFT in both $[Pb(PYTAM)]^{2+}$ and $[Pb(H_4PYTAMGly)]^{2+}$ indicates that the Pb(II) lone pair has a 100% 6s character (Table S1, ESI†). This is in line with the general trend that holodirected structures are favoured by the presence of neutral donor atoms and high coordination numbers.[51]

The conformation of the macrocycles in these complexes is similar to those observed for lanthanide complexes based on the same macrocycle and functionalised with identical pendant arms.[53–57] Two pendant arms attached to opposite N atoms on the macrocyclic structure are placed above the mean plane defined by the pyridine rings, while the remaining two pendant arms are placed below that plane. This conformation, together with the symmetrical coordination environment imposes a $D_2$ symmetry for the $[Pb(PYTAM)]^{2+}$ complex. Fig. 1 shows views of the structure of this complex along the three perpendicular $C_2$ axes characterising the $D_2$ point group. The five-membered chelates generated upon coordination of the ethylenediamine spacers adopt the same conformations, which can be represented as ($\lambda\lambda$) or ($\delta\delta$) (Fig. S3, ESI†).[58,59] Furthermore, the four amine N atoms adopt identical configurations. The two structures are centrosymmetric, with both ($\lambda\lambda$)-*RRRR* and ($\delta\delta$)-*SSSS* enantiomers being present in the crystal.

### Solution structure of the Pb(II) complexes

The Pb(II) complexes of the four chelators were prepared *in situ* by adding $Pb(NO_3)_2$ to a solution of the chelator in $D_2O$. Upon addition of the metal salt, the pD dropped to low values, between 1 and 2. While $^1$H-NMR of the complexes with ethylene spacers show one species in solution, the complexes with cyclohexyl spacers do not show one unique species, presenting more complex spectra, at this pD (Fig. S4, ESI†). The pD was then raised to ~7 using NaOD to record the NMR spectra of the complexes (Fig. 2).

The $^1$H NMR spectra of the four complexes are characteristic of highly rigid structures, as evidenced by the well-resolved signals that can be observed in the aliphatic region, where doublets corresponding to AB systems associated with the geminal coupling of the protons of the $CH_2$ groups appear (Fig. 2). These characteristic doublets are easily identified through their large $^2J$ values (~15 Hz) and roof effect. This is due to the rigidity of the system, which locks the protons of these groups into specific positions, making them no longer chemically equivalent. The NMR data in solution indicate the presence of a single complex species in each case. The number

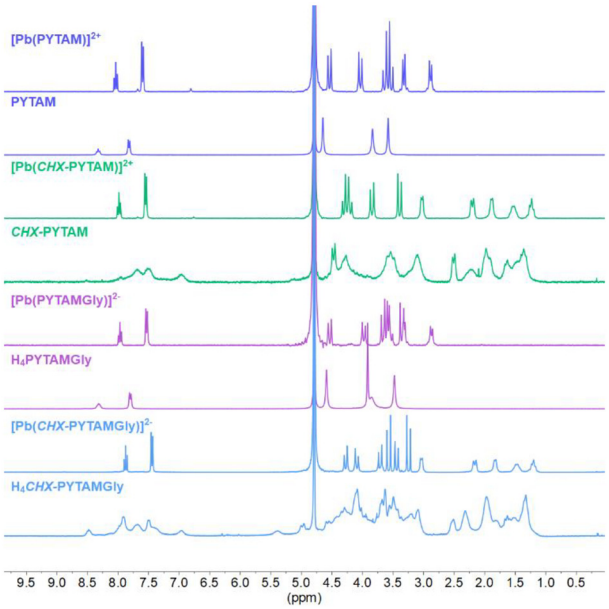


**Fig. 2** $^1$H NMR spectra of $[Pb(PYTAM)]^{2+}$ (pD = 6.5), PYTAM (pD = 1.4) $[Pb(CHX\text{-}PYTAM)]^{2+}$ (pD = 7.4), *CHX*-PYTAM (pD = 1.7), $[Pb(PYTAMGly)]^{2-}$ (pD = 6.8), $H_4$PYTAMGly (pD = 2.0), $[Pb(CHX\text{-}PYTAMGly)]^{2+}$ (pD = 6.3) and $H_4CHX$-PYTAMGly (pD = 2.0), recorded in $D_2O$ solution (300 MHz, 298 K).

of $^1$H and $^{13}$C NMR signals point to an effective $D_2$ symmetry of the complexes in solution. A full assignment of the $^1$H and $^{13}$C NMR spectra, achieved with the aid of 2D COSY, HSQC and HMBC experiments, along with *J* coupling values, is provided in the ESI (Tables S2–S4†). Noteworthy, the $^1$H NMR spectra of the free PYTAM and $H_4$PYTAMGly chelators are characteristic of flexible molecules, with the signals due to $CH_2$ groups being observed as singlets. The $^1$H NMR spectra of the corresponding cyclohexyl derivatives display broad signals, which reflects a certain degree of rigidity of the free chelator in solution.

Additional information on the structures of the complexes in solution was obtained from 2D $^1$H–$^{207}$Pb heteronuclear multiple-quantum correlation (HMQC) spectra (Fig. 3).[60] These spectra provide two strong cross-peaks relating the $^{207}$Pb resonance and the equatorial protons of the methylenic groups of the molecule (H4 and H5, see Scheme 1). Additionally, another strong cross peak is observed for one of the signals of the $CH_2$ protons of the ethylene spacer (H7) in $[Pb(PYTAM)]^{2+}$ and $[Pb(PYTAMGly)]^{2-}$. The set of three geminal (axial) $CH_2$ signals provide however weak cross peaks. This indicates that axial and equatorial protons provide rather different $^3J_{Pb-H}$ coupling constants. Furthermore, the axial C–H protons (H7) of the cyclohexyl group in $[Pb(CHX\text{-}PYTAM)]^{2+}$ and $[Pb(CHX\text{-}PYTAMGly)]^{2-}$ do not provide cross peaks with the $^{207}$Pb nucleus. Thus, we conclude that equatorial protons give much stronger cross peaks in the HMQC spectra than the axial counterparts. Equatorial $CH_2$ protons are characterised by H–C–N–Pb dihedral angles of ~160–170°, while axial protons give

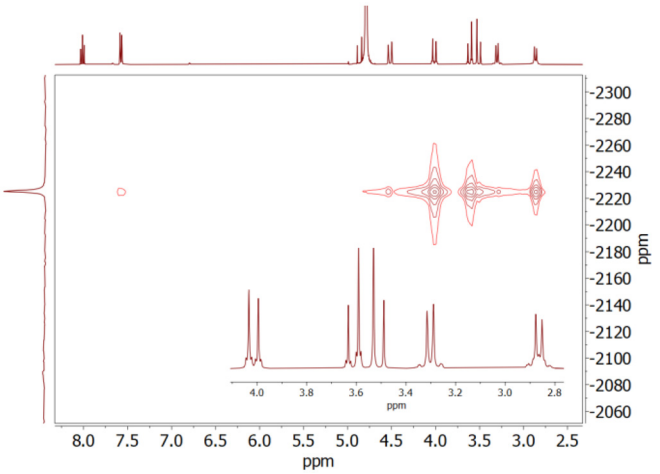


**Fig. 3** $^{1}$H–$^{207}$Pb HMQC spectrum of [Pb(PYTAM)]$^{2+}$ (pD = 6.5) recorded in $D_2O$ solution (400 MHz, 298 K). The inset shows an expansion of the aliphatic region where satellites due to $^{3}J(^{1}H–^{207}Pb)$ coupling are evident.

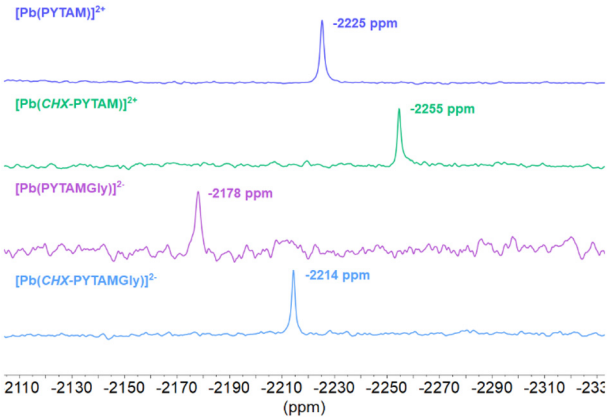


**Fig. 4** $^{207}$Pb NMR spectra of [Pb(PYTAM)]$^{2+}$ (pD = 6.5), [Pb(*CHX*-PYTAM)]$^{2+}$ (pD = 7.4), [Pb(PYTAMGly)]$^{2-}$ (pD = 6.8), [Pb(*CHX*-PYTAMGly)]$^{2+}$ (pD = 6.3) recorded in $D_2O$ solution (84 MHz, 298 K).

dihedral angles of ~70–80°. This suggests that the $^{3}J_{Pb–H}$ coupling constants involving methylenic protons follow a Karplus-like relationship with the dihedral H–C–N–Pb angle,[61] as observed previously for properties originated by through-bond effects (*i.e.* spin densities).[62] The strong $^{3}J_{Pb–H}$ coupling involving equatorial protons is also evident by the presence of satellites in the $^{1}$H NMR spectra (Fig. 3) due to coupling with $^{207}$Pb ($I = \frac{1}{2}$), which has a 22.6% natural abundance. These satellites provide $^{3}J(^{1}H–^{207}Pb)$ couplings of ~8–9 Hz, which are in the low range reported for Pb(II) complexes containing H–C–N($sp^3$) bonds (*ca.* 8–20 Hz).[60,63] Larger coupling constants of up to ~43 Hz were reported for $^{3}J(^{1}H–^{207}Pb)$ couplings involving $sp^2$ N donor atoms.[64–66] Nevertheless, the presence of the $^{3}J(^{1}H–^{207}Pb)$ coupling constants confirms the coordination of the macrocyclic unit to the Pb(II) ion and reveals a certain degree of covalence of the Pb–$N_{amine}$ bonds. We also notice that the pyridyl protons H2 give a sizeable $^{4}J(^{1}H–^{207}Pb)$ coupling of ~3 Hz, pointing to a rather strong coordination of the pyridyl N atom to the metal ion.

The $^{207}$Pb NMR spectra of the complexes display signals in the range −2178 to −2255 ppm, with the cyclohexyl derivatives providing slightly more negative chemical shifts and the glycinate derivatives slightly more positive shifts (Fig. 4). The similar $\delta$ values observed for the four complexes point to comparable Pb(II) coordination environments. The $^{207}$Pb NMR signals observed here are shielded by ~4000 ppm with respect to those reported for EDTA derivatives[60,67] and [Pb(DOTAM)]$^{2+}$.[68] Positive chemical shift values were also reported for complexes with crown ether derivatives[64] (the chemical shift of neat $Pb(CH_3)_4$ used as a reference corresponds to +2961 ppm *versus* the 1 M aqueous $Pb(NO_3)_2$ reference used here).[67] The negative $\delta$ values found for the ten-coordinated Pb(II) ions reported here follow the general trend of an increasing shielding with higher coordination numbers.[69] A similar situation was observed for Y(III) complexes, as ten-coordinated derivatives displayed unusually shielded $^{89}$Y resonances.[70] In the latter case the experimental $^{89}$Y shifts could be approximated by the sum of the shielding contributions of the chelator donor atoms, and thus an increased coordination number results in a more important shielding effect. A similar behaviour may affect the $^{207}$Pb NMR shifts, though investigation of a wider range of complexes is required to find correlations between the number and type of donor atoms and the observed shifts.

### Protonation constants and thermodynamic stability of the Pb(II) complexes of the glycinate derivatives

The protonation constants of the chelators and the stability constants of the lead(II) complexes were determined for the glycinate derivatives, as the chelators containing acetamide pendants presented solubility issues in basic media. Chelator protonation constants were measured using potentiometric and spectrophotometric titrations, following the absorption of the pyridyl groups at *ca.* 265 nm. Potentiometric titrations afforded three protonation constants for PYTAMGly$^{4-}$ above pH 5.0 and up to four protonation constants with log $K$ values in the range ~2.4 to 4.1. The assignment of the protonation constants was aided by spectrophotometric titrations (Fig. 5). Indeed, the absorption spectrum recorded at pH 1.30 displays a maximum at 263 nm and a shoulder at 267 nm. Increasing the pH above ~4.0 provokes a slight shift of the absorption maximum to 265 nm as the band becomes more rounded and its intensity decreases. These spectral changes are compatible with the protonation of a pyridyl unit.[34] The log $K$ value obtained from spectrophotometric titrations (4.98) is in very good agreement with that determined by potentiometry (log $K_3$ = 5.11(1)). The spectrum experiences further changes above pH ~ 5.6, with the absorption maximum experiencing a slight shift to lower energies (267 nm) as its intensity increases. Spectrophotometric titrations afforded a single protonation constant of log $K$ = 6.29(1), which coincides with the average of log $K_1$ (6.70(1)) and log $K_2$ (5.88(1)) obtained by potentiometry.

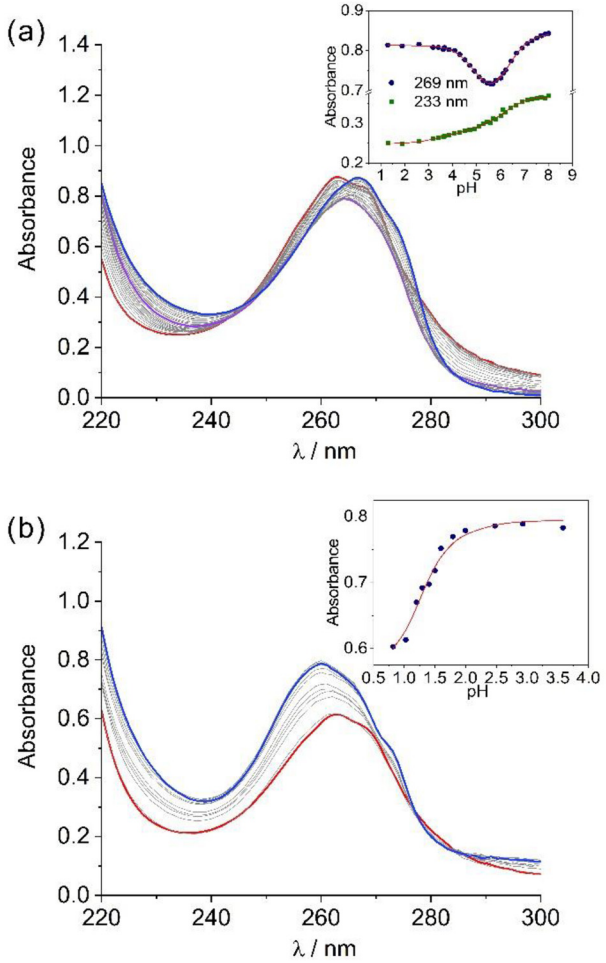


**Fig. 5** (a) UV-Vis absorption spectra recorded for a solution of PYTAMGly$^{4-}$ ($10^{-4}$ M, $I$ = 0.15 M $NaClO_4$, 25 °C) at different pH values. The spectra highlighted in red, violet, and blue correspond to pH values of 1.30, 5.57 and 8.01, respectively. The inset shows the spectral changes at selected wavelengths and the fits of the data. (b) UV-Vis absorption spectra recorded to monitor the dissociation of the pre-formed Pb(II) complex with PYTAMGly$^{4-}$ ($10^{-4}$ M, $I$ = 0.15 M $NaClO_4$, 25 °C) at different pH values. The spectra highlighted in red, and blue correspond to pH values of 0.82 and 3.58, respectively. The inset shows the spectral changes at 261 nm and the fit of the data.

We therefore assign these protonation constants to the amine groups of the macrocycle, though the significant spectral changes suggest that the pyridine units are also involved in these protonation processes. A comparison of the protonation constants $\log K_1$ and $\log K_2$ determined for PYTAMGly$^{4-}$ and DOTAMGly$^{4-}$ indicate that the amine groups of the 12-membered CYCLEN ring are considerably more basic than those of the 18-membered ring of PYTAMGly$^{4-}$. The 18-membered macrocycle crown-4Py displays an intermediate behaviour.[15] The protonation constants determined for PYAN using 0.1 M $KNO_3$ and 0.1 M KCl as background electrolytes evidence that the incorporation of the amide pendants in PYTAMGly$^{4-}$ considerably reduces the basicity of the N atoms of the macrocycle (Table 2).[71–73]

The protonation constants $\log K_4$–$\log K_7$ determined by potentiometry are not associated to noticeable spectral changes in the absorption spectra, and therefore can be safely assigned to the remote glycinate groups. Similar protonation constants were reported for the glycinate groups of DOTAMGly$^{4-}$.[74] The protonation of four non-interacting carboxylates is expected to have statistical separations of $\Delta\log K$ = 0.42, 0.36 and 0.42. The experimental protonation constants yield $\Delta\log K_{4,5}$ = 0.62, $\log K_{5,6}$ = 0.33 and $\log K_{6,7}$ = 0.67, in reasonable agreement with the values expected according to the statistical factor.[75,76]

The same combined methodology was used to determine the protonation constants of *CHX*-PYTAMGly$^{4-}$. The constants involving the protonation of amine groups, $\log K_1$ and $\log K_2$, are about 2 $\log K$ units higher than those determined for PYTAMGly$^{4-}$ (Table 2). This is expected, as in general the substitution of ethyl for cyclohexyl groups significantly increases chelator basicity.[31,77] The protonation constants $\log K_3$–$\log K_6$ are attributed to the protonation of the glycinate groups on the basis of the minor spectral changes observed in the absorption spectra (Fig. S6, ESI†). These protonation constants follow again reasonably well the trend expected according to the statistical factor. Interestingly, spectrophotometric experiments demonstrate that the protonation of the pyridine ring occurs at low pH, with a protonation constant of $\log K_7$ = 2.05(9). The rigidity of the macrocycle introduced by the presence of cyclohexyl rings appears to be responsible for the sharp decrease in the protonation constant of the pyridyl unit.

The stability constants of the Pb(II) complexes with PYTAMGly$^{4-}$ and *CHX*-PYTAMGly$^{4-}$ were determined using a combination of potentiometric and spectrophotometric titrations. Potentiometry was used to obtain the protonation constants of the complexes, while complex dissociation was investigated spectrophotometrically following the changes in the absorption band of the pyridyl groups. Of note, the amount of free Pb(II) at pH ~2 is only 1.5 and 6.5% for PYTAMGly$^{4-}$ and *CHX*-PYTAMGly$^{4-}$, respectively, preventing the determination of stability constants by direct potentiometry. The absorption band of the pyridyl rings of PYTAMGly$^{4-}$ at 263 nm undergoes a slight blue shift to 260 nm as its intensity increases as a result of complex formation (Fig. 5b). Similar spectral variations are observed for *CHX*-PYTAMGly$^{4-}$ (Fig. S6, ESI†). The fits of the data afforded the stability and protonation constants shown in Table 2. These studies showed that the incorporation of the cyclohexyl spacer did not have a large effect on the value of $\log K_{PbL}$ affording values of 17.03 and 17.17 for $[Pb(H_4PYTAMGly)]^{2-}$ and $[Pb(H_4CHX\text{-}PYTAMGly)]^{2-}$, respectively. These values are higher than those reported for the complexes with other potentially decadentate 18-membered macrocycles such as MACROPA$^{2-}$ and crown-4Py.[15,78] Higher stability constants were reported for CYCLEN derivatives containing pyridyl rings such as CYCLEN-4Py.[15] However, the low basicity of PYTAMGly$^{4-}$ and especially *CHX*-PYTAMGly$^{4-}$ renders rather high conditional stability at physiological pH. This can be conveniently assessed by calculating pPb values, defined as $-\log [Pb(II)]_{free}$ for a metal ion concentration of 1 μM and a total

 

**Table 2** Chelator protonation constants and stability constants of Pb(II) complexes ($I$ = 0.15 M $NaClO_4$, 25 °C)

| | PYTAMGly$^{4-}$ | *CHX*-PYTAMGly$^{4-}$ | MACROPA$^{2-}$ [a] | Cyclen-4Py[b] | Crown-4Py[b] | DOTAMGly$^{4-}$ [c] | PYAN[d] |
|---|---|---|---|---|---|---|---|
| $\log K_1$ | 6.70(1) | 8.69(5) | 7.52 | 10.05 | 7.91 | 9.19 | 8.99 |
| $\log K_2$ | 5.88(1) | 7.80(7) | 7.03 | 7.53 | 7.33 | 6.25 | 8.22 |
| $\log K_3$ | 5.11(1) | 4.38(9) | 3.58 | 3.54 | 4.64 | 4.08 | 6.03 |
| $\log K_4$ | 4.08(1) | 3.66(9) | 2.47 | 2.23 | 4.00 | 3.45 | 5.34 |
| $\log K_5$ | 3.46(1) | 3.31(9) | | | | 3.20 | 2.11 |
| $\log K_6$ | 3.13(1) | 2.62(9) | | | | 1.40 | |
| $\log K_7$ | 2.46(1) | 2.05(9) | | | | | |
| $\log K_{PbL}$ | 17.03(1) | 17.18(1) | 16.23 | 19.95 | 13.29 | | |
| $\log K_{PbHL}$ | 4.58(2) | 4.691(2) | 2.86 | 2.06 | 5.22 | | |
| $\log K_{PbH_2L}$ | 3.57(4) | 3.66(7) | | | 3.50 | | |
| $\log K_{PbH_3L}$ | 3.49(4) | 3.52(8) | | | | | |
| $\log K_{PbH_4L}$ | 2.87(3) | 3.09(6) | | | | | |
| pPb | 17.9 | 16.3 | 16.7 | 17.88 | 13.40 | | |

[a] Data from ref. 78, 0.1 M $KNO_3$, 25 °C. [b] Data from ref. 15, 0.1 M KCl, 25 °C. [c] Data from ref. 74, 0.1 M KCl, 25 °C. [d] Data from ref. 71, 0.1 M $KNO_3$, 25 °C.

chelator concentration of 10 μM.[79] The pPb values obtained for PYTAMGly$^{4-}$ and CYCLEN-4py are virtually identical in spite of the three orders of magnitude difference in stability constants. The pPb value calculated for *CHX*-PYTAMGly$^{4-}$ is nearly two units lower than that of PYTAMGly$^{4-}$ as a result of the lower basicity of the latter, though comparable to that of MACROPA$^{2-}$.

The speciation diagrams calculated from equilibrium constants (Fig. 6) indicate that complex protonation takes place below pH ~ 7, with the non-protonated complex species being at nearly 100% abundance around neutral pH. Complex dissociation occurs below pH ~ 2 and pH ~ 3 for PYTAMGly$^{4-}$ and *CHX*-PYTAMGly$^{4-}$, respectively. The two complexes show a very similar protonation behaviour, with four protonation constants associated to the glycinate groups. The $\Delta\log K_{PbHL,PbH_2L}$ values of 1.01 and 1.03 for the complexes with PYTAMGly$^{4-}$ and *CHX*-PYTAMGly$^{4-}$, respectively, are higher than that expected according to the statistical effect (0.42), while the values of $\Delta\log K_{PbH_2L,PbH_3L} < 0.15$ are lower than the statistical value of 0.36.[76] This suggests a certain negative cooperativity for the formation of the deprotonated complex species. We also note that the glycinate groups are characterized by higher protonation constants in the complexes compared with the free ligands. Complex formation forces the negatively charged glycinate groups to be in rather close proximity (Fig. 1), which likely favours their protonation.

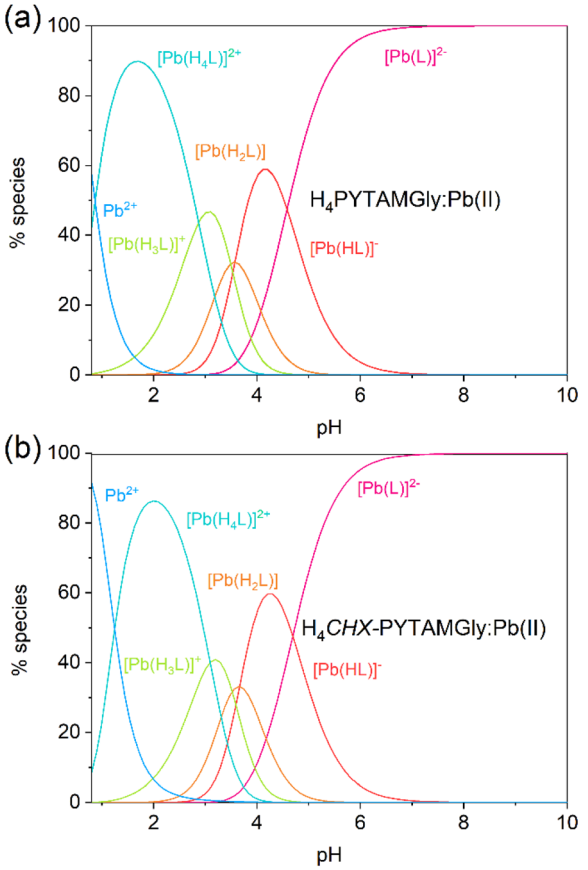


**Fig. 6** Speciation diagrams of the $H_4$PYTAMGly:Pb(II) (a) and $H_4$*CHX*-PYTAMGly$^{4-}$:Pb(II) (b) systems calculated for $[Pb(II)]_{tot}$ = $[L]_{tot}$ = 1 mM (25 °C, $I$ = 0.15 M $NaClO_4$).

## Radiolabelling studies

Once the non-radioactive studies showed that these chelators presented appropriate properties for Pb(II) complexation, lead-203 radiolabelling studies were performed. [$^{203}$Pb]Pb(II) was produced and purified according to the procedure reported by McNeil *et al.*, without any modifications.[80] Concentration dependent radiolabelling for all four chelators and DOTAM, the gold-standard for radiolabelling with lead(II) isotopes, was performed in $NH_4OAc$ buffer (0.1 M, pH 7) at five different chelator concentrations ($10^{-4}$, $10^{-5}$, $10^{-6}$, $10^{-7}$ and $10^{-8}$ M). The reactions were followed at two time points (30 and 60 minutes) and two temperatures (room temperature: ~25 °C, and 80 °C). The radiochemical yields (RCYs) were determined by spotting an aliquot of the reaction onto iTLC-SA plates and developed using 50 mM EDTA (pH 5) as the mobile phase.

The RCYs observed for both temperatures at 60 min (Fig. 7 and Tables S4, S5, ESI†) improve slightly with respect to those

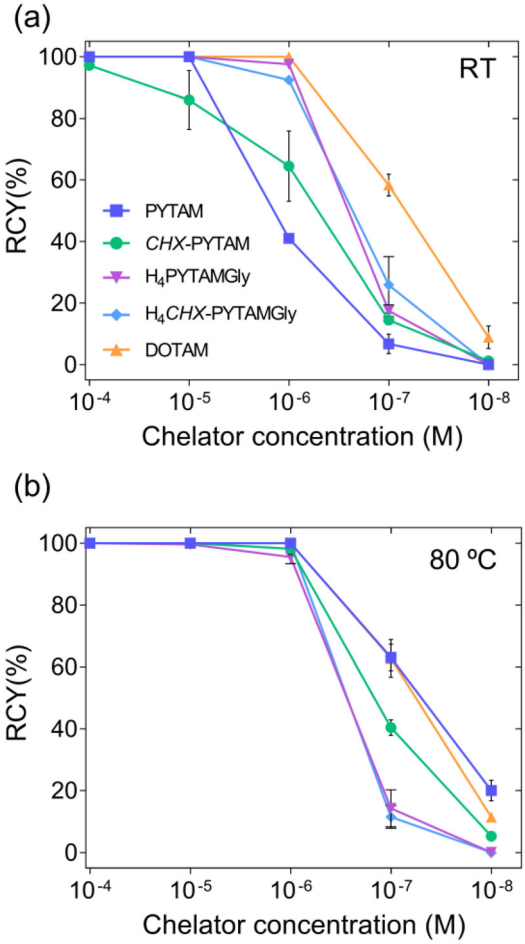


**Fig. 7** Radiolabelling studies using $^{203}$Pb (~150 kBq, 0.1 M $NH_4OAc$ buffer, pH 7) ($n$ = 3 for each data point). (a) Concentration dependent radiolabelling at room temperature after 60 min. (b) Concentration dependent radiolabelling at 80 °C after 60 min.

recorded at 30 min (Fig. S8 and Tables S6, S7 ESI†). At room temperature (Fig. 7a and Table S5, ESI†), *CHX*-PYTAM is the only chelator that does not reach quantitative yields at $10^{-4}$ M, although the RCY is still high with a value of 97.2 ± 1.2% at this concentration. This effect is most likely due to the rigidity introduced by the cyclohexyl spacers, since at higher temperatures the yields are superior. At 80 °C (Fig. 7b and Table S6, ESI†), the RCYs of PYTAM and *CHX*-PYTAM are comparable to the values observed for DOTAM. The glycinate derivatives, however, behave differently, and their RCYs do not improve significantly as the labelling efficiency of these chelators is nearly identical at both room temperature and 80 °C.

Since $^{203}$Pb-radiolabelling of *CHX*-PYTAM at room temperature was not fully quantitative at the highest chelator concentration, labelling of this chelator was also performed at 37 °C (Table S9, ESI†), in addition to room temperature (~25 °C) and 80 °C (Fig. 8). The radiochemical yields improve significantly at this temperature for all concentrations, with yields of nearly 100% for both $10^{-4}$ and $10^{-5}$ M (98.4 ± 0.4 and 97.3 ± 0.5%, respectively) after 30 minutes and even higher yields after

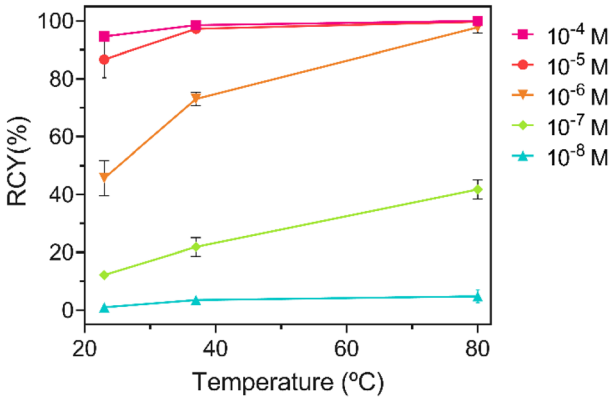


**Fig. 8** Temperature dependent $^{203}$Pb-radiolabelling (150 kBq, 0.1 M $NH_4OAc$ buffer, pH 7, 30 min) of *CHX*-PYTAM at different concentrations ($n$ = 3 for each data point).

60 min (100% and 99.6 ± 0.6%, respectively). This result indicates that although labelling of 100% was not achieved at room temperature, the system is still quite promising for the design of bifunctional systems, as heating to 37 °C is still compatible with most biological targeting vectors.

Once the $^{203}$Pb-labelled complexes were prepared, challenge experiments were performed to assess the kinetic inertness of the $^{203}$Pb complexes. The complexes were formed at either room temperature and/or 80 °C to be representative of the tested radiolabelling conditions (Fig. 9 and Fig. S9, Tables S10–S14, ESI†). The purpose of this experiment was to evaluate the influence of complexation temperature on stability. For the stable Pb(II) and EDTA challenges, 20 equivalents of the respective chemical was added to the radiolabelling solution. DOTAM forms incredibly stable complexes in the studied competitive media, remaining 100% intact in all the conditions investigated. The complexes formed with PYTAM, $H_4$PYTAMGly, and *CHX*-PYTAM presented excellent stability in presence of 20 equiv. of EDTA (Fig. 9b) over the course of over one half-life, showing no indications of transchelation. However, $H_4$*CHX*-PYTAMGly did not remain intact, neither when prepared at room temperature or 80 °C. It may be possible that the steric hindrance introduced by the simultaneous presence of cyclohexyl spacer and acetylglycine pendant arms facilitates transchelation.

When incubated with excess (20 equiv.) of stable Pb(II) (Fig. 9c), *CHX*-PYTAM is the only chelator that forms a complex that is stable under these conditions. The complex is 100% intact after 24 hours and after 72 hours the majority (93.2 ± 0.4%) of the radiocomplex remains intact. $H_4$PYTAMGly is the least stable as within 2 hours, only 13.4 ± 2.0% of the complex remained intact at this time point. PYTAM and $H_4$*CHX*-PYTAMGly, while not as stable as *CHX*-PYTAM, performed better than $H_4$PYTAMGly, with similar results, as 37.0 ± 2.0% and 54.3 ± 1.5% of the complex is stable after 72 hours, respectively. It is surprising, after seeing the results of the competition with $H_4$EDTA, that $H_4$*CHX*-PYTAMGly performed better than $H_4$PYTAMGly under these conditions, though

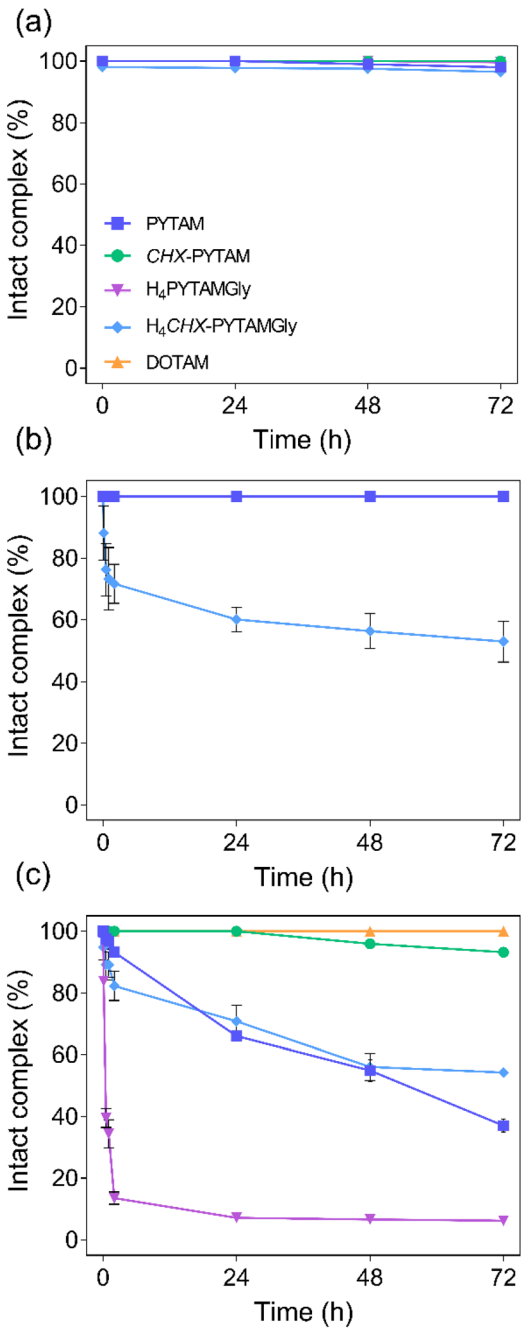


**Fig. 9** Challenging studies of the $^{203}$Pb-labelled complexes (150 kBq, 0.1 M $NH_4OAc$ buffer, pH 7) ($n$ = 3 for each data point). (a) Human serum stability challenge. (b) Excess EDTA challenge (20 equiv.). (c) Excess stable Pb(II) challenge (20 equiv.).

transchelation and transmetallation occur through different mechanisms. The presence of glycinate groups likely favours the formation of the dinuclear intermediate responsible for the Pb(II)-assisted dissociation mechanism. The high stability of *CHX*-PYTAM is most likely due to the increase in rigidity introduced by the two cyclohexyl groups in the backbone and the use of acetamide pendant arms, which appears to be the ideal combination for complex stability. It should be noted though that the complex formed with DOTAM does, in fact, remain 100% stable. However, the 93.2 ± 0.4% of intact complex, observed for *CHX*-PYTAM at 72 hours, is the highest of all of the chelators presented in this work, and it should not present any issues *in vivo* as high concentrations of Pb(II) are not expected to be found in the body.

Finally, the kinetic inertness of the complexes was evaluated when incubated in human serum at 37 °C (Fig. 9a). *CHX*-PYTAM showed no dissociation over 72 hours while the other three chelators did drop slightly but remained above 95% in all cases. These results point towards all four complexes possibly being stable under *in vivo* conditions, although further studies would be necessary to confirm this hypothesis.

## Conclusions

We have shown that macrocyclic chelators based on the 18-membered platform PYAN show promising properties for the development of Pb-based radiopharmaceuticals. Stable Pb(II) complexation was achieved by incorporating four amide pendant arms, leading to the formation of stable and rigid complexes with ten-coordinated Pb(II) ions. The inertness of the complexes is improved by incorporating rigid cyclohexyl spacers into the macrocyclic ring. The presence of bulky acetylglycine pendant arms appears to introduce some steric hindrance, while the chelator *CHX*-PYTAM displays excellent properties for the development of Pb-based radiopharmaceuticals. We are currently developing bifunctional derivatives of this platform to be able to further study the potential of these chelates.

## Experimental section

### General considerations

Solvents and reagents were purchased from commercial sources and were used as supplied without further purification. Medium performance liquid chromatography (MPLC) was performed in a Puriflash XS 420 InterChim Chromatographer equipped with a UV-DAD detector and a 20 g BGB Aquarius C18AQ reversed-phase column (100 Å, spherical, 15 μm) using $H_2O$ and $CH_3CN$ with 0.1% TFA as the mobile phases. Semi-preparative high performance liquid chromatography (HPLC) was performed using a Jasco LC-4000 instrument equipped with a UV-4075 detector, in manual injection and collection mode, using a Fortis C18 column (5μm, 250 × 10 mm) and $H_2O$ and $CH_3CN$ with 0.1% TFA as the mobile phases, operating at a flow rate of 4.0 mL min$^{-1}$. High-resolution electrospray-ionization time-of-flight ESI-TOF mass spectra were recorded in positive mode using a LTQ-Orbitrap Discovery Mass Spectrometer coupled to a Thermo Accela HPLC. $^1$H and $^{13}$C NMR spectra of the chelators and their complexes were recorded on Bruker AVANCE III 300, Bruker AVANCE 400 or Bruker AVANCE 500 spectrometers. PYAN (3,6,10,13-tetraaza-1,8(2,6)-dipyridinacyclotetradeca-

phane), *tert*-butyl (2-chloroacetyl)glycinate and PYTAM (2,2′,2″,2‴-(3,6,10,13-tetraaza-1,8(2,6)-dipyridinacyclotetradecaphane-3,6,10,13-tetrayl)tetraacetamide) were prepared according to previously reported procedures.[45,81,82]

### 2,2′,2″,2‴-((2,2′,2″,2‴-(3,6,10,13-Tetraaza-1,8(2,6)-dipyridinacyclotetradecaphane-3,6,10,13-tetrayl)tetrakis(acetyl))tetrakis(azanediyl))tetraacetic acid ($H_4$PYTAMGly)

PYAN (0.1869 g, 0.57 mmol), $K_2CO_3$ (0.4734 g, 3.43 mmol) and KI (0.0095 g, 0.057 mmol) were added to $CH_3CN$ (40 mL) while the mixture was heated to 50 °C. *tert*-Butyl (2-chloroacetyl)glycinate (0.5920 g, 2.85 mmol) was dissolved in $CH_3CN$ (15 mL) and added dropwise over the course of 2 hours after which the reaction was left stirring at 50 °C for 6 days after which the solvent was eliminated in the rotary evaporator. The product was isolated by suspending the oil in $H_2O$ (50 mL) and performing extractions with $CHCl_3$ (3 × 50 mL). The organic phase was separated, dried using $Na_2SO_4$, and concentrated in the rotary evaporator. A yellow oil was obtained after drying in the vacuum line, which is dissolved in 20 mL of a 1 : 1 TFA : $CH_2Cl_2$ mixture and left stirring overnight. The solvent was then eliminated under a nitrogen flow and was washed with water (3 × 15 mL), obtaining a brown oil. This oil was dissolved in water (1.5 mL) and was purified by reverse phase using method A (Table S15†). The desired compound eluted at 36% $CH_3CN$ (retention time 8.6 min, 6.3 CV). The fraction of interest was lyophilized and an off-white solid was obtained (0.0887 g, 13% yield). $^1$H NMR (300 MHz, $D_2O$, pD 2.0) $\delta$ (ppm) 8.31 (s, br, 2H), 7.80 (d, $J$ = 7.4 Hz, 4H), 4.59 (s, 8H), 3.92 (s, 8 H), 3.85 (s, br, 8H), 3.48 (s, 8H).$^{13}$C NMR (75 MHz, $D_2O$, pD 2.0) $\delta$ (ppm) 172.96, 169.33, 150.57, 126.03, 55.12, 52.00, 41.15. Elemental analysis calcd (%) for $C_{34}H_{46}N_{10}O_{12}$·4TFA: C 40.59, H 4.06, N 11.27; found: C 40.68, H 4.35, N 11.35. Experimental MS (ESI$^+$, MeOH/$H_2O$): *m*/*z* 413.1459, 424.1364, 825.2847; calculated for $[C_{34}H_{47}N_{10}O_{12}K]^{2+}$ 413.1501, calculated for $[C_{34}H_{47}N_{10}O_{12}NaK]^{2+}$ 424.1410, calculated for $[C_{34}H_{46}N_{10}O_{12}K]^+$ 825.2928.

### ($4^1R$,$4^2R$,$10^1R$,$10^2R$)-3,5,9,11-Tetraaza-1,7(2,6)-dipyridina-4,10(1,2)-dicyclohexanacyclododecaphane (*CHX*-PYAN)

Synthesis adapted from a previously reported procedure.[47] Pyridine-2,6-dicarbaldehyde (0.6250 g, 4.63 mmol) was dissolved in MeOH (150 mL) along with barium chloride dihydrate (0.4830 g, 2.32 mmol). (1*R*,2*R*)-Cyclohexane-1,2-diamine (0.5281 g, 4.62 mmol) was dissolved in MeOH (10 mL) and added dropwise to the refluxing reaction mixture over the course of 2 hours. The reaction was then left heating for an additional 3 hours after which it was cooled to 0 °C in an ice bath and $NaBH_4$ (0.2122 g, 6.07 mmol) was added in small increments. The reaction mixture was allowed to reach room temperature, a second addition of $NaBH_4$ (0.1062 g, 3.02 mmol) was made and the reaction was left stirring for 3 hours. The solvent was then eliminated in the rotary evaporator and water (50 mL, pH adjusted to 9 using NaOH) was added. Extractions with $CHCl_3$ (3 × 50 mL) (50 mL) were performed and the combined organic phases were dried using $NaSO_4$, filtered and concentrated in the rotary evaporator, obtaining a yellow solid (1.2429 g, yield 87%). $^1$H NMR (500 MHz, $CDCl_3$) $\delta$ (ppm) 7.55 (s, 2H), 7.04 (d, $^3J$ = 7.6 Hz, 4H), 4.10 (d, $^2J$ = 15.4 Hz, 4H), 3.80 (d, $^2J$ = 15.7 Hz, 5H), 2.17–1.95 (m, 8H), 1.63 (d, $^2J$ = 7.3 Hz, 4H), 1.18–0.96 (m, 8H). $^{13}$C NMR (126 MHz, $CDCl_3$) $\delta$ 137.19, 121.63, 59.56, 32.97, 24.99. Elemental analysis calcd (%) for $C_{26}H_{38}N_6$·1.65$CHCl_3$: C 52.64, H 6.23, N 12.97; found: C 52.58, H 6.33, N 13.31. Experimental MS (ESI$^+$, MeOH/$H_2O$): *m*/*z* 435.3206, 457.3022; calculated for $[C_{26}H_{39}N_6]^+$ 435.3231, calculated for $[C_{26}H_{39}N_6Na]^+$ 457.3050.

### 2,2′,2″,2‴-((($4^1R$,$4^2R$,$10^1R$,$10^2R$)-3,5,9,11-Tetraaza-1,7(2,6)-dipyridina-4,10(1,2)-dicyclohexanacyclododecaphane-3,5,9,11-tetrayl)tetraacetamide (*CHX*-PYTAM)

*CHX*-PYAN·1.65$CHCl_3$ (0.3008 g, 0.484 mmol) was dissolved in $CH_3CN$ (20 mL) and $Na_2CO_3$ (0.3204 g, 3.02 mmol) was added. 2-Bromoacetamide (0.2689 g, 1.95 mmol) was dissolved in $CH_3CN$ (10 mL) and added dropwise over the course of an hour. After stirring for three days, the solvent was evaporated, and the resulting yellow solid was then prepared for purification by MPLC. The solid was dissolved in water (1 mL) by lowering the pH to pH = 3 using HCl. This solution was purified by reverse phase using method B (Table S16†), and the desired compound eluted at 27% $CH_3CN$ (retention time 12.2 min, 8.9 CV). The fraction of interest was lyophilized and an off-white solid was obtained (180.0 mg, 40% yield). $^1$H NMR (400 MHz, $D_2O$, pD = 1.74, 343.15 K) $\delta$ (ppm) 8.26 (s, 2H), 7.99 (d, $^3J$ = 5.9 Hz, 2H), 7.60 (s, 2H), 5.19–4.85 (m, 3H), 4.69 (d, $^2J$ = 15.3 Hz, 2H), 4.47 (d, $^2J$ = 14.6 Hz, 2H), 4.17–3.75 (m, 5H), 3.60 (d, $^2J$ = 13.6 Hz, 4H), 2.97 (d, $^2J$ = 10.6 Hz, 2H), 2.83–2.56 (m, 2H), 2.53–2.29 (m, 4H), 2.09 (d, $^2J$ = 10.1 Hz, 2H), 1.98–1.70 (m, 6H).$^{13}$C NMR (101 MHz, $D_2O$, pD = 1.74, 343.15 K) $\delta$ (ppm) 174.07, 169.61, 157.17, 151.74, 140.35, 126.54, 126.51, 123.26 (br), 62.93 (br), 61.57 (br), 58.33, 54.46 (br), 52.97, 52.28, 24.39, 24.14. Elemental analysis calcd (%) for $C_{34}H_{50}N_{10}O_4$·1.5TFA·1.5HBr: C 46.52, H 5.59, N 14.66; found: C 46.46, H 5.61, N 14.72. Experimental MS (ESI$^+$, MeOH/$H_2O$): *m*/*z* 332.2083, 663.4094, 685.3912; calculated for $[C_{34}H_{52}N_{10}O_4]^{2+}$ 332.2081, calculated for $[C_{34}H_{51}N_{10}O_4]^+$ 663.4089, calculated for $[C_{34}H_{50}N_{10}O_4K]^+$ 685.3909.

### 2,2′,2″,2‴-((2,2′,2″,2‴-((($4^1R$,$4^2R$,$10^1R$,$10^2R$)-3,5,9,11-Tetraaza-1,7(2,6)-dipyridina-4,10(1,2)-dicyclohexanacyclododecaphane-3,5,9,11-tetrayl)tetrakis(acetyl))tetrakis(azanediyl))tetraacetic acid ($H_4$*CHX*-PYTAMGly)

*CHX*-PYAN·$(CHCl_3)_{1.65}$ (0.2000 g, 0.32 mmol), $K_2CO_3$ (0.3890 g, 2.81 mmol) and *tert*-butyl (2-chloroacetyl)glycinate (0.3920 g, 1.89 mmol) were added to $CH_3CN$ (30 mL) and left stirring at room temperature for 30 days, following the progress of the reaction using mass spectrometry. After this time, since the reaction was not evolving to form the tetraalkylated derivative, more *tert*-butyl (2-chloroacetyl)glycinate (0.0294 g, 0.14 mmol) was added, and the reaction was left stirring for another 30 days after which the solvent was concentrated in the rotary evaporator and the product was isolated by adding $CHCl_3$

 

(30 mL) and $H_2O$ with the pH adjusted to 9 using NaOH (30 mL) and performing an additional two extractions with $CHCl_3$ (30 mL). The organic phase was separated, dried using $Na_2SO_4$, and concentrated in the rotary evaporator. A yellow oil was obtained after drying in the vacuum line, which was dissolved in 10 mL of a 1 : 1 TFA : $CH_2Cl_2$ mixture and left stirring overnight. The solvent was then eliminated under a nitrogen flow and was washed with water (3 × 15 mL), obtaining a brown oil. This oil was dissolved in water (1.5 mL) and was purified by reverse phase using method C (Table S17†). The desired compound eluted at 41% $CH_3CN$ (retention time 12.4 min, 9.1 CV). The fraction of interest was lyophilized, and a white solid was obtained (185.6 mg, 44% yield). $^1$H NMR (400 MHz, $D_2O$, pD = 10.2, 343.15 K) $\delta$ (ppm) 8.02 (t, $^3J$ = 7.7 Hz, 2H), 7.64 (d, $^3J$ = 7.5 Hz, 4H), 4.33–3.43 (m, 16H), 3.22 (s, 4H), 2.51 (d, $^2J$ = 10.0 Hz, 4H), 2.28–1.99 (m, 5H), 1.76–1.37 (m, 6H).$^{13}$C NMR (101 MHz, $D_2O$, pD = 10.2, 343.15 K) $\delta$ (ppm) 176.34, 161.69, 158.74, 139.19, 123.26, 43.60, 25.67, 25.01. Elemental analysis calcd (%) for $C_{42}H_{58}N_{10}O_{12}$·3.5TFA·2$H_2O$: C 44.25, H 4.96, N 10.53; found: C 44.02, H 4.71, N 10.76. Experimental MS (ESI$^+$, MeOH/$H_2O$): *m*/*z* 448.2192, 895.4324, 917.4142; calculated for $[C_{42}H_{60}N_{10}O_{12}]^{2+}$ 448.2191, calculated for $[C_{42}H_{59}N_{10}O_{12}]^+$ 895.4308, calculated for $[C_{42}H_{58}N_{10}O_{12}K]^+$ 917.4128.

### General procedure for the synthesis of the lead complexes

The Pb(II) complexes were prepared *in situ* by adding $Pb(NO_3)_2$ to a solution of each chelator in deuterated water (0.5 mL) in a molar ratio of 1 : 1.1 ($H_4$L: $Pb(NO_3)_2$). At this point, the mixture was quite acidic so the pD is adjusted above pD = 6 using a diluted solution of NaOD while the formation of the complex was monitored using NMR.

### Crystal structure determination

Compounds **[Pb(PYTAM)](PF$_6$)$_2$** and **[Pb(H$_4$PYTAMGly)](NO$_3$)$_2$** were analysed by X-ray diffraction. Table S19† shows the crystallographic data and structure refinement parameters. Crystallographic data were collected on a Bruker D8 Venture diffractometer with a Photon 100 CMOS detector at 100 K with Mo-Kα radiation ($\lambda$ = 0.71073 Å) generated by an Incoatec high brilliance microfocus source equipped with Incoatec Helios multilayer optics. The APEX4[83] software was used for collecting frames of data, indexing reflections, and the determination of lattice parameters, while SAINT[84] was used for integration of intensity of reflections, and SADABS[85] for scaling and empirical absorption correction. The structure was solved by dual-space methods using the program SHELXT.[86] All non-hydrogen atoms were refined with anisotropic thermal parameters by full-matrix least-squares calculations on $F^2$ using the program SHELXL-2014.[87] Hydrogen atoms were inserted at calculated positions and constrained with isotropic thermal parameters. The crystal structure of [Pb($H_4$PYTAMGly)]($NO_3$)$_2$ shows a B level Alert in the checkcif due a short distance between two hydrogen atoms: one belonging to a water molecule (H5WA) and the other to a protonated glycinate group (H2A). The protonated glycinate group shows hydrogen bond interaction with the water molecule. Also, H5WA shows a hydrogen bond interaction with one nitrate group. These interactions determine the position of the hydrogens. CCDC 2305213 and 2305214 contain the supplementary crystallographic data.†

### Potentiometric and spectrophotometric measurements

Stability constants and chelator protonation constants were determined through potentiometric and spectrophotometric titrations using HYPERQUAD.[88] All data were collected at 25 °C and $NaClO_4$ was used as an inert electrolyte which is added to all solutions to maintain the ionic strength at a constant value of $I$ = 0.15 M.

Potentiometric titrations were carried out in dual-wall thermostated cell, using recirculating water. Nitrogen was bubbled on the surface to avoid $CO_2$ absorption and the solutions were homogenised using magnetic stirring. The titrant was added using a Crison microBu 2030 automatic burette and the electromotive force (emf) was recorded using a Crison micropH 2000 pH meter connected to a Radiometer pHG211 glass electrode and a Radiometer REF201 reference electrode. A 1 mM solution of the chelator (10 mL) was added to the cell, and the pH of the solution was adjusted to 11 using NaOH. This solution was then titrated using a standard $HClO_4$ solution to determine all p$K_a$ values in the same experiment. Once the solution reached an acidic pH, an equimolar amount of Pb(II) was added and the mixture was left stirring for one hour to ensure complex formation. The solution was titrated with a solution of NaOH to determine the protonation constants of the complex. At this point it became clear that the stability constant of the complex must be determined by spectrophotometry, as the dissociation occurs at pH values that are too low to be determined using the glass electrode.

To determine equilibrium constants, HYPERQUAD calculates the proton concentration at each point of the titration using emf values, $E$, and using the electrode calibration equation, $E = E^{o\prime} + s\log[H^+]$, with $E^{o\prime}$ representing the formal potential and s, the slope of the electrode. Both parameters are determined with a calibration of the electrode system, conducted by titrating $HClO_4$ with NaOH, both with known concentrations and adjusted ionic strength, as $[H^+]$ is known for each calibration point and $E$ is measured, with a lineal regression giving the values of $E^{o\prime}$ and $s$.

Spectrophotometric titrations were performed using a Uvikon-XS (Bio-Tek Instruments) double-beam spectrophotometer and 1 cm path length quartz cuvettes, recording spectra between 220 and 300 nm. The spectra of each chelator at concentrations between 6–10 × $10^{-5}$ M at different pH values were used to obtain the p$K_a$ values of the chelators. The desired pH was obtained using different buffers (acetate, phosphate, borax) and for very low pH values, $HClO_4$ was used directly (*i.e.* stability constant determination). Dissociation of the complexes was achieved at low pH values, and although equilibrium is reached quite quickly, the samples were equilibrated for a few hours before each measurement.

The ligand protonation constants reported in this work are defined as in eqn (1), where L represents a general ligand:

$$K_i = \frac{[H_iL]}{[H_{i-1}L][H^+]} \quad (1)$$

The stability constants of the Pb(II) complexes and their protonation constants are defined as in eqn (2) and (3), respectively.

$$K_{PbL} = \frac{[PbL]}{[Pb][L]} \quad (2)$$

$$K_{PbH_iL} = \frac{[PbH_iL]}{[PbH_{i-1}L][H^+]} \quad (3)$$

### DFT calculations

DFT calculations were performed with the Gaussian 16 program package,[89] with the TPSSh functional and the Def2-TZVPP basis set for chelator atoms. For Pb, we selected the small-core relativistic effective core potential of Dolg *et al.* (ECP60MDF),[90] which incorporates 60 electrons in the core, together with the cc-pVTZ valence basis set, which has a (12s11p8d1f)/[5s4p3d1f] contraction scheme.[91] Calculations were performed using crystallographic structures in which only the positions of H atoms were optimised. The integration grid was set with the integral = ultrafinegrid keyword. Natural bond orbital analysis was carried out with the NBO program (version 3.1)[92] included in Gaussian.

### Radiolabelling

**Caution**: $^{203}$Pb emits ionizing radiation and should only be used in a facility in accordance with appropriate safety controls.

All chelators were purified by HPLC before radiolabelling experiments to ensure high purity (Table S18, ESI†).

Stock solutions, with a concentration of $10^{-3}$ M of DOTAM, PYTAM, $H_4$PYTAMGly, *CHX*-PYTAM and $H_4$*CHX*-PYTAMGly were prepared in deionized water. Serial dilution was then used to prepare chelator solutions with concentrations between $10^{-4}$ M and $10^{-7}$ M. For the $^{203}$Pb labelling studies, a 10 μL aliquot of chelator (or deionized water for the negative control) was added to 78 μL of deionized water and 10 μL of 1 M $NH_4OAc$ (pH 7) and 2 μL of [$^{203}$Pb]$Pb(Cl)_2$ (150 kBq) were added and mixed to begin the reactions, which were performed in triplicate and left at either room temperature or 80 °C until measurement at 30 and 60 minutes. iTLC was used to determine radiochemical yields (RCY) of the reactions, using iTLC-SA (iTLC paper impregnated with silicic acid) plates (1.5 × 10 cm, baseline at 1.5 cm; Agilent Technologies), developed using 50 mM EDTA (pH 5). With this system, complexed $^{203}$Pb(II) remained at the baseline ($R_f$ = 0) while uncomplexed $^{203}$Pb(II) migrated at the solvent front ($R_f$ = 1) (representative iTLCs are included in ESI, Fig. S10–S16†). Aliquots of the reactions were taken at 30 and 60 min, spotted onto the plates, and developed. RCYs were then measured using a BioScan System 200 Scanner (Washington, DC) and quantified with WinScan software.

### Human serum stability studies

The stability of the five radiocomplexes was determined by adding 90 μL of human serum to previously radiolabelled solutions ($10^{-4}$ M chelator concentration, 90 μL) and the resulting mixture was incubated at 37 °C. Aliquots (10 μL) were taken at 24, 48 and 72 hours and spotted onto the iTLC-SA plates, developed, and then analysed using the previously reported procedure, to determine the amount of intact complex.

### EDTA and Pb(II) challenging studies

Stock solutions of EDTA (pH = 7) and $Pb(OAc)_2$ were prepared with a concentration of 20 mM. Preformed $^{203}$Pb-complexes ($10^{-4}$ M chelator concentration, 100 μL volume), prepared both at room temperature and 80 °C, were then challenged with a 20-fold excess of either EDTA or Pb(II) as 10 μL of the 20 mM solution was added to the radiolabelling reaction. Aliquots (10 μL) were taken at 0.083, 0.5, 1, 2, 24, 48 and 72 hours and spotted onto the iTLC-SA plates, which were then analysed using the previously reported procedure, to evaluate the inertness of the complexes.

## Author contributions

The manuscript was written through contributions of all authors. All authors have given approval to the final version of the manuscript.

## Conflicts of interest

There are no conflicts to declare.

## Acknowledgements

D. E.-G. and C. P.-I. thank Ministerio de Ciencia e Innovación (Grants PID2019-104626GB-I00 and PID2022-138335NB-I00) and Xunta de Galicia (ED431C 2023/33) for generous financial support. C. H. thanks Ministerio de Ciencia e Innovación (Grant PRE2020-092888) for funding her PhD contract and a short-term research visit to SFU and TRIUMF. C. P.-I. and C. H. thank Centro de Supercomputación de Galicia (CESGA) for providing supercomputer facilities. L. V. is indebted to CACTI (Universidade de Vigo) for X-ray measurements. C. F. R and B. L. M thank the Natural Sciences and Engineering Research Council (NSERC) of Canada for funding through the Discovery grants (RGPIN-2019-07207) and Canada Graduate Scholarships – Doctoral (CGS-D) programs, respectively. B. L. M thanks the TRIUMF cyclotron operators for their continued support with $^{203}$Pb production at TRIUMF. Funding for open access provided by Universidade da Coruña/CISUG.

 

## References

1 T. I. Kostelnik and C. Orvig, Radioactive Main Group and Rare Earth Metals for Imaging and Therapy, *Chem. Rev.*, 2019, **119**, 902–956.
2 S. L. Pimlott and A. Sutherland, Molecular tracers for the PET and SPECT imaging of disease, *Chem. Soc. Rev.*, 2010, **40**, 149–162.
3 D. E. Milenic and M. W. Brechbiel, Targeting of Radio-Isotopes for Cancer Therapy, *Cancer Biol. Ther.*, 2004, **3**, 361–370.
4 L. Filippi, A. Chiaravalloti, O. Schillaci, R. Cianni and O. Bagni, Theranostic approaches in nuclear medicine: current status and future prospects, *Expert Rev. Med. Devices*, 2020, **17**, 331–343.
5 N. H. Álvarez, D. Bauer, J. Hernández-Gil and J. S. Lewis, Recent Advances in Radiometals for Combined Imaging and Therapy in Cancer, *ChemMedChem*, 2021, **16**, 2909–2941.
6 C. Miller, J. Rousseau, C. F. Ramogida, A. Celler, A. Rahmim and C. F. Uribe, Implications of physics, chemistry and biology for dosimetry calculations using theranostic pairs, *Theranostics*, 2022, **12**, 232–259.
7 S. R. Banerjee, V. Kumar, A. Lisok, J. Chen, I. Minn, M. Brummet, S. Boinapally, M. Cole, E. Ngen, B. Wharram, C. Brayton, R. F. Hobbs and M. G. Pomper, 177Lu-labeled low-molecular-weight agents for PSMA-targeted radiopharmaceutical therapy, *Eur. J. Nucl. Med. Mol. Imaging*, 2019, **46**, 2545–2557.
8 C. Kim, S. V. Liu, D. S. Subramaniam, T. Torres, M. Loda, G. Esposito and G. Giaccone, Phase I study of the $^{177}$Lu-DOTA$^{0}$-Tyr$^{3}$-Octreotate (lutathera) in combination with nivolumab in patients with neuroendocrine tumors of the lung, *J. Immunother. Cancer*, 2020, **8**, e000980.
9 T. Rold, N. Okoye, E. Devanny, A. Berendzen, T. Dresser, T. Quinn and T. Hoffman, Pb-203/Pb-212 Evaluation as Theranostic Pair for Prostate Cancer Detection, Monitoring, and Treatment, *J. Nucl. Med.*, 2020, **61**, 229–229.
10 B. L. McNeil, A. K. H. Robertson, W. Fu, H. Yang, C. Hoehr, C. F. Ramogida and P. Schaffer, Production, purification, and radiolabeling of the 203Pb/212Pb theranostic pair, *EJNMMI Radiopharm. Chem.*, 2021, **6**, 6.
11 C. G. Pippin, T. J. McMurry, M. W. Brechbiel, M. McDonald, R. Lambrecht, D. Milenic, M. Roselli, D. Colcher and O. A. Gansow, Lead(II) complexes of 1,4,7,10-tetraazacyclododecane-N,N′,N″,N‴-tetraacetate: solution chemistry and application to tumor localization with 203Pb labeled monoclonal antibodies, *Inorg. Chim. Acta*, 1995, **239**, 43–51.
12 L. L. Chappell, E. Dadachova, D. E. Milenic, K. Garmestani, C. Wu and M. W. Brechbiel, Synthesis, characterization, and evaluation of a novel bifunctional chelating agent for the lead isotopes 203Pb and 212Pb, *Nucl. Med. Biol.*, 2000, **27**, 93–100.
13 A. Ingham, L. Wharton, T. El Sayed, L. Southcott, B. L. McNeil, M. B. Ezhova, B. O. Patrick, M. de G. Jaraquemada-Peláez and C. Orvig, H2ampa–Versatile Chelator for [203Pb]Pb2+, [213Bi]Bi3+, and [225Ac]Ac3+, *Inorg. Chem.*, 2022, **61**, 9119–9137.
14 A. Ingham, T. I. Kostelnik, B. L. McNeil, B. O. Patrick, N. Choudhary, M. de G. Jaraquemada-Peláez and C. Orvig, Getting a lead on Pb2+-amide chelators for 203/212Pb radiopharmaceuticals, *Dalton Trans.*, 2021, **50**, 11579–11595.
15 B. L. McNeil, K. J. Kadassery, A. W. McDonagh, W. Zhou, P. Schaffer, J. J. Wilson and C. F. Ramogida, Evaluation of the Effect of Macrocyclic Ring Size on [203Pb]Pb(II) Complex Stability in Pyridyl-Containing Chelators, *Inorg. Chem.*, 2022, **61**, 9638–9649.
16 B. J. B. Nelson, J. Wilson, M. K. Schultz, J. D. Andersson and F. Wuest, High-yield cyclotron production of 203Pb using a sealed 205Tl solid target, *Nucl. Med. Biol.*, 2023, **116–117**, 108314.
17 R. G. Li, V. Y. Stenberg and R. H. Larsen, An Experimental Generator for Production of High-Purity 212Pb for Use in Radiopharmaceuticals, *J. Nucl. Med.*, 2023, **64**, 173–176.
18 S. R. Banerjee, I. Minn, V. Kumar, A. Josefsson, A. Lisok, M. Brummet, J. Chen, A. P. Kiess, K. Baidoo, C. Brayton, R. C. Mease, M. Brechbiel, G. Sgouros, R. F. Hobbs and M. G. Pomper, Preclinical Evaluation of $^{203/212}$Pb-Labeled Low-Molecular-Weight Compounds for Targeted Radiopharmaceutical Therapy of Prostate Cancer, *J. Nucl. Med.*, 2020, **61**, 80–88.
19 J. C. dos Santos, M. Schäfer, U. Bauder-Wüst, W. Lehnert, K. Leotta, A. Morgenstern, K. Kopka, U. Haberkorn, W. Mier and C. Kratochwil, Development and dosimetry of 203Pb/212Pb-labelled PSMA ligands: bringing "the lead" into PSMA-targeted alpha therapy?, *Eur. J. Nucl. Med. Mol. Imaging*, 2019, **46**, 1081–1091.
20 E. S. Delpassand, I. Tworowska, R. Esfandiari, J. Torgue, J. Hurt, A. Shafie and R. Núñez, Targeted α-Emitter Therapy with 212Pb-DOTAMTATE for the Treatment of Metastatic SSTR-Expressing Neuroendocrine Tumors: First-in-Humans Dose-Escalation Clinical Trial, *J. Nucl. Med.*, 2022, **63**, 1326–1333.
21 M. W. Brechbiel, Bifunctional Chelates for Metal Nuclides, *Q. J. Nucl. Med. Mol. Imaging*, 2008, **52**, 166–173.
22 E. W. Price and C. Orvig, Matching chelators to radiometals for radiopharmaceuticals, *Chem. Soc. Rev.*, 2014, **43**, 260–290.
23 K. Zukotynski, H. Jadvar, J. Capala and F. Fahey, Targeted Radionuclide Therapy: Practical Applications and Future Prospects: Supplementary Issue: Biomarkers and their Essential Role in the Development of Personalised Therapies (A), *Biomarkers Cancer*, 2016, **8s2**, BIC.S31804.
24 E. Boros, B. V. Marquez, O. F. Ikotun, S. E. Lapi and C. L. Ferreira, in *Ligand Design in Medicinal Inorganic Chemistry*, John Wiley & Sons, Ltd, 2014, pp. 47–79.
25 R. G. Pearson, Hard and Soft Acids and Bases, *J. Am. Chem. Soc.*, 1963, **85**, 3533–3539.
26 H. Maumela, R. D. Hancock, L. Carlton, J. H. Reibenspies and K. P. Wainwright, The Amide Oxygen as a Donor

Group. Metal Ion Complexing Properties of Tetra-N-acetamide Substituted Cyclen: A Crystallographic, NMR, Molecular Mechanics, and Thermodynamic Study, *J. Am. Chem. Soc.*, 1995, **117**, 6698–6707.

27 R. Hancock, Macrocyclic ligands with pendent amide and alcoholic oxygen donor groups, *Coord. Chem. Rev.*, 1996, **148**, 315–347.

28 R. Delgado, V. Félix, L. M. P. Lima and D. W. Price, Metal complexes of cyclen and cyclam derivatives useful for medical applications: a discussion based on thermodynamic stability constants and structural data, *Dalton Trans.*, 2007, 2734–2745.

29 T. J. Clough, L. Jiang, K.-L. Wong and N. J. Long, Ligand design strategies to increase stability of gadolinium-based magnetic resonance imaging contrast agents, *Nat. Commun.*, 2019, **10**, 1420.

30 R. D. Hancock and A. E. Martell, Ligand design for selective complexation of metal ions in aqueous solution, *Chem. Rev.*, 1989, **89**, 1875–1914.

31 C. F. Ramogida, J. F. Cawthray, E. Boros, C. L. Ferreira, B. O. Patrick, M. J. Adam and C. Orvig, H2 CHX dedpa and H4 CHX octapa-Chiral acyclic chelating ligands for 67/68Ga and 111In radiopharmaceuticals, *Inorg. Chem.*, 2015, **54**, 2017–2031.

32 F. Lucio-Martínez, Z. Garda, B. Váradi, F. K. Kálmán, D. Esteban-Gómez, É. Tóth, G. Tircsó and C. Platas-Iglesias, Rigidified Derivative of the Non-macrocyclic Ligand $H_4$ OCTAPA for Stable Lanthanide(III) Complexation, *Inorg. Chem.*, 2022, **61**, 5157–5171.

33 F. Lucio-Martínez, D. Esteban-Gómez, L. Valencia, D. Horváth, D. Szücs, A. Fekete, D. Szikra, G. Tircsó and C. Platas-Iglesias, Rigid H4OCTAPA derivatives as model chelators for the development of Bi(III)-based radiopharmaceuticals, *Chem. Commun.*, 2023, **59**, 3443–3446.

34 R. Uzal-Varela, D. Lalli, I. Brandariz, A. Rodríguez-Rodríguez, C. Platas-Iglesias, M. Botta and D. Esteban-Gómez, Rigid versions of PDTA4− incorporating a 1,3-diaminocyclobutyl spacer for Mn2+ complexation: stability, water exchange dynamics and relaxivity, *Dalton Trans.*, 2021, **50**, 16290–16303.

35 N. A. Thiele, J. J. Woods and J. J. Wilson, Implementing f-Block Metal Ions in Medicine: Tuning the Size Selectivity of Expanded Macrocycles, *Inorg. Chem.*, 2019, **58**, 10483–10500.

36 G. J. Stasiuk and N. J. Long, The ubiquitous DOTA and its derivatives: the impact of 1,4,7,10-tetraazacyclododecane-1,4,7,10-tetraacetic acid on biomedical imaging, *Chem. Commun.*, 2013, **49**, 2732.

37 R. E. Mewis and S. J. Archibald, Biomedical applications of macrocyclic ligand complexes, *Coord. Chem. Rev.*, 2010, **254**, 1686–1712.

38 A. Hu, E. Aluicio-Sarduy, V. Brown, S. N. MacMillan, K. V. Becker, T. E. Barnhart, V. Radchenko, C. F. Ramogida, J. W. Engle and J. J. Wilson, Py-Macrodipa: A Janus Chelator Capable of Binding Medicinally Relevant Rare-Earth Radiometals of Disparate Sizes, *J. Am. Chem. Soc.*, 2021, **143**, 10429–10440.

39 A. Hu, V. Brown, S. N. MacMillan, V. Radchenko, H. Yang, L. Wharton, C. F. Ramogida and J. J. Wilson, Chelating the Alpha Therapy Radionuclides 225Ac3+ and 213Bi3+ with 18-Membered Macrocyclic Ligands Macrodipa and Py-Macrodipa, *Inorg. Chem.*, 2022, **61**, 801–806.

40 N. A. Thiele, V. Brown, J. M. Kelly, A. Amor-Coarasa, U. Jermilova, S. N. MacMillan, A. Nikolopoulou, S. Ponnala, C. F. Ramogida, A. K. H. Robertson, C. Rodríguez-Rodríguez, P. Schaffer, C. Williams Jr., J. W. Babich, V. Radchenko and J. J. Wilson, An Eighteen-Membered Macrocyclic Ligand for Actinium-225 Targeted Alpha Therapy, *Angew. Chem., Int. Ed.*, 2017, **56**, 14712–14717.

41 K. J. Kadassery, A. P. King, S. Fayn, K. E. Baidoo, S. N. MacMillan, F. E. Escorcia and J. J. Wilson, H2BZmacropa-NCS: A Bifunctional Chelator for Actinium-225 Targeted Alpha Therapy, *Bioconjugate Chem.*, 2022, **33**, 1222–1231.

42 C. Harriswangler, L. Caneda-Martínez, O. Rousseaux, D. Esteban-Gómez, O. Fougère, R. Pujales-Paradela, L. Valencia, M. I. Fernández, N. Lepareur and C. Platas-Iglesias, Versatile Macrocyclic Platform for the Complexation of [natY/90Y]Yttrium and Lanthanide Ions, *Inorg. Chem.*, 2022, **61**, 6209–6222.

43 H. Yang, C. Zhang, Z. Yuan, C. Rodriguez-Rodriguez, A. Robertson, V. Radchenko, R. Perron, D. Gendron, P. Causey, F. Gao, F. Bénard and P. Schaffer, Synthesis and Evaluation of a Macrocyclic Actinium-225 Chelator, Quality Control and In Vivo Evaluation of 225Ac-crown-αMSH Peptide, *Chem. – Eur. J.*, 2020, **26**, 11435–11440.

44 L. Wharton, S. W. McNeil, H. Merkens, Z. Yuan, M. Van de Voorde, G. Engudar, A. Ingham, H. Koniar, C. Rodríguez-Rodríguez, V. Radchenko, M. Ooms, P. Kunz, F. Bénard, P. Schaffer and H. Yang, Preclinical Evaluation of [155/161Tb]Tb-Crown-TATE—A Novel SPECT Imaging Theranostic Agent Targeting Neuroendocrine Tumours, *Molecules*, 2023, **28**, 3155.

45 T. Gambino, L. Valencia, P. Pérez-Lourido, D. Esteban-Gómez, M. Zaiss, C. Platas-Iglesias and G. Angelovski, Inert macrocyclic Eu $^{3+}$ complex with affirmative paraCEST features, *Inorg. Chem. Front.*, 2020, **7**, 2274–2286.

46 G. Castro, G. Wang, T. Gambino, D. Esteban-Gómez, L. Valencia, G. Angelovski, C. Platas-Iglesias and P. Pérez-Lourido, Lanthanide(III) Complexes Based on an 18-Membered Macrocycle Containing Acetamide Pendants. Structural Characterization and paraCEST Properties, *Inorg. Chem.*, 2021, **60**, 1902–1914.

47 P. M. Michelle and S. C. Jackels, Helical hexaazamacrocyclic ligands containing pyridyl and (+ or −)-trans-diaminocyclohexyl groups: effect of ligand constraints upon metal ion binding, *Inorg. Chim. Acta*, 1996, **246**, 301–310.

48 L. M. P. Lima, M. Beyler, R. Delgado, C. Platas-Iglesias and R. Tripier, Investigating the Complexation of the $Pb^{2+}$ /$Bi^{3+}$ Pair with Dipicolinate Cyclen Ligands, *Inorg. Chem.*, 2015, **54**, 7045–7057.

 

49 R. D. Hancock, J. H. Reibenspies and H. Maumela, Structural Effects of the Lone Pair on Lead(II), and Parallels with the Coordination Geometry of Mercury(II). Does the Lone Pair on Lead(II) Form H-Bonds? Structures of the Lead(II) and Mercury(II) Complexes of the Pendant-Donor Macrocycle DOTAM (1,4,7,10-Tetrakis(carbamoylmethyl)-1,4,7,10-tetraazacyclododecane), *Inorg. Chem.*, 2004, **43**, 2981–2987.

50 J. W. Nugent, H.-S. Lee, J. H. Reibenspies and R. D. Hancock, Spectroscopic, structural, and thermodynamic aspects of the stereochemically active lone pair on lead(II): Structure of the lead(II) dota complex, *Polyhedron*, 2015, **91**, 120–127.

51 L. Shimoni-Livny, J. P. Glusker and C. W. Bock, Lone Pair Functionality in Divalent Lead Compounds, *Inorg. Chem.*, 1998, **37**, 1853–1867.

52 D. Esteban-Gómez, C. Platas-Iglesias, T. Enríquez-Pérez, F. Avecilla, A. De Blas and T. Rodríguez-Blas, Lone-Pair Activity in Lead(II) Complexes with Unsymmetrical Lariat Ethers, *Inorg. Chem.*, 2006, **45**, 5407–5416.

53 S. W. A. Bligh, N. Choi, C. F. G. C. Geraldes, S. Knoke, M. McPartlin, M. J. Sanganee and T. M. Woodroffe, A novel hexaaza macrocycle with methylenephosphonate pendant arms: a potential useful chelate for biomedical applications †, *J. Chem. Soc., Dalton Trans.*, 1997, 4119–4126.

54 L. Valencia, J. Martinez, A. Macías, R. Bastida, R. A. Carvalho and C. F. G. C. Geraldes, X-ray Diffraction and $^{1}$H NMR in Solution: Structural Determination of Lanthanide Complexes of a $Py_2N_6Ac_4$ Ligand, *Inorg. Chem.*, 2002, **41**, 5300–5312.

55 G. Castro, G. Wang, T. Gambino, D. Esteban-Gómez, L. Valencia, G. Angelovski, C. Platas-Iglesias and P. Pérez-Lourido, Lanthanide(III) Complexes Based on an 18-Membered Macrocycle Containing Acetamide Pendants. Structural Characterization and paraCEST Properties, *Inorg. Chem.*, 2021, **60**, 1902–1914.

56 G. Castro, M. Regueiro-Figueroa, D. Esteban-Gómez, R. Bastida, A. Macías, P. Pérez-Lourido, C. Platas-Iglesias and L. Valencia, Exceptionally Inert Lanthanide(III) PARACEST MRI Contrast Agents Based on an 18-Membered Macrocyclic Platform, *Chem. – Eur. J.*, 2015, **21**, 18662–18670.

57 M. del C. Fernández-Fernández, R. Bastida, A. Macías, P. Pérez-Lourido, C. Platas-Iglesias and L. Valencia, Lanthanide(III) Complexes with a Tetrapyridine Pendant-Armed Macrocyclic Ligand: 1 H NMR Structural Determination in Solution, X-ray Diffraction, and Density-Functional Theory Calculations, *Inorg. Chem.*, 2006, **45**, 4484–4496.

58 E. J. Corey and J. C. Bailar, The Stereochemistry of Complex Inorganic Compounds. XXII. Stereospecific Effects in Complex Ions [1], *J. Am. Chem. Soc.*, 1959, **81**, 2620–2629.

59 J. K. Beattie, Conformational analysis of tris(ethylenediamine) complexes, *Acc. Chem. Res.*, 1971, **4**, 253–259.

60 E. S. Claudio, M. A. ter Horst, C. E. Forde, C. L. Stern, M. K. Zart and H. A. Godwin, $^{207}$Pb– $^{1}$H Two-Dimensional NMR Spectroscopy: A Useful New Tool for Probing Lead(II) Coordination Chemistry, *Inorg. Chem.*, 2000, **39**, 1391–1397.

61 M. Karplus, Vicinal Proton Coupling in Nuclear Magnetic Resonance, *J. Am. Chem. Soc.*, 1963, **85**, 2870–2871.

62 A. Rodríguez-Rodríguez, D. Esteban-Gómez, A. de Blas, T. Rodríguez-Blas, M. Botta, R. Tripier and C. Platas-Iglesias, Solution Structure of Ln(III) Complexes with Macrocyclic Ligands Through Theoretical Evaluation of $^{1}$H NMR Contact Shifts, *Inorg. Chem.*, 2012, **51**, 13419–13429.

63 M. Regueiro-Figueroa, D. Esteban-Gómez, C. Platas-Iglesias, A. De Blas and T. Rodríguez-Blas, Metal Ion Complementarity: Effect of Ring–Size Variation on the Conformation and Stability of Lead(II) and Cadmium(II) Complexes with Pendant–Armed Crowns, *Eur. J. Inorg. Chem.*, 2007, **2007**, 2198–2207.

64 D. Esteban-Gómez, R. Ferreirós, S. Fernández-Martínez, F. Avecilla, C. Platas-Iglesias, A. De Blas and T. Rodríguez-Blas, Lateral Macrobicyclic Architectures: Toward New Lead (II) Sequestering Agents, *Inorg. Chem.*, 2005, **44**, 5428–5436.

65 D. Esteban, F. Avecilla, C. Platas-Iglesias, J. Mahía, A. de Blas and T. Rodríguez-Blas, Lead(II) Complexes with Macrocyclic Receptors Derived from 4,13-Diaza-18-crown-6, *Inorg. Chem.*, 2002, **41**, 7170–7170.

66 D. Esteban, F. Avecilla, C. Platas-Iglesias, J. Mahía, A. de Blas and T. Rodríguez-Blas, Lead(II) Complexes with Macrocyclic Receptors Derived from 4,13-Diaza-18-crown-6, *Inorg. Chem.*, 2002, **41**, 4337–4347.

67 J. Sanchiz, P. Esparza, D. Villagra, S. Domínguez, A. Mederos, F. Brito, L. Araujo, A. Sánchez and J. M. Arrieta, Holo- and Hemidirected Lead(II) in the Polymeric $[Pb_4(\mu\text{-}3,4\text{-}TDTA)_2(H_2O)_2]\cdot 4H_2O$ Complex. *N*,*N*,*N*′,*N*′-Tetraacetate Ligands Derived from *o*-Phenylenediamines as Sequestering Agents for Lead(II), *Inorg. Chem.*, 2002, **41**, 6048–6055.

68 F. Cuenot, M. Meyer, E. Espinosa, A. Bucaille, R. Burgat, R. Guilard and C. Marichal-Westrich, New Insights into the Complexation of Lead(II) by 1,4,7,10-Tetrakis(carbamoylmethyl)-1,4,7,10-tetraazacyclododecane (DOTAM): Structural, Thermodynamic, and Kinetic Studies, *Eur. J. Inorg. Chem.*, 2008, **2008**, 267–283.

69 B. Wrackmeyer and K. Horchler, in *Annual Reports on NMR Spectroscopy*, Elsevier, 1990, vol. 22, pp. 249–306.

70 Y. Xing, A. K. Jindal, M. Regueiro-Figueroa, M. Le Fur, N. Kervarec, P. Zhao, Z. Kovacs, L. Valencia, P. Pérez-Lourido, R. Tripier, D. Esteban-Gómez, C. Platas-Iglesias and A. D. Sherry, The Relationship between NMR Chemical Shifts of Thermally Polarized and Hyperpolarized $^{89}$Y Complexes and Their Solution Structures, *Chem. – Eur. J.*, 2016, **22**, 16657–16667.

71 L. Branco, J. Costa, R. Delgado, M. G. B. Drew, V. Félix and B. J. Goodfellow, Metal complexes of dipyridine hexaaza macrocycles. Structural differences between 18- and 20-membered macrocycles on complexation, *J. Chem. Soc., Dalton Trans.*, 2002, 3539–3550.

72 K. I. Dhont, G. G. Herman, A. C. Fabretti, W. Lippens and A. M. Goeminne, Protonation and metal-ion complexation

in aqueous solution by pyridine-containing hexaaza macrocycles, *J. Chem. Soc., Dalton Trans.*, 1996, 1753.

73 C. Cruz, S. Carvalho, R. Delgado, M. G. B. Drew, V. Félix and B. J. Goodfellow, Metal complexes of a dipyridine octaazamacrocycle: stability constants, structural and modelling studies, *Dalton Trans.*, 2003, 3172–3183.

74 Z. Baranyai, E. Brücher, T. Iványi, R. Király, I. Lázár and L. Zékány, Complexation Properties of *N*,*N*′,*N*″,*N*‴,-[1,4,7,10-Tetraazacyclododecane-1,4,7,10-tetrayltetrakis(1-oxoethane-2,1-diyl)]tetrakis[glycine] ($H_4$dotagl). Equilibrium, Kinetic, and Relaxation Behavior of the Lanthanide(III) Complexes, *Helv. Chim. Acta*, 2005, **88**, 604–617.

75 E. Graf, J. Harrowfield, J. Kintzinger, J. Lehn, J. Le Moigne and K. Rissanen, Protonation of a Spherical Macrotricyclic Tetramine: Water Inclusion, Allosteric Effect, and Cooperativity, *ChemPlusChem*, 2018, **83**, 605–611.

76 J. Hamacek, M. Borkovec and C. Piguet, Simple thermodynamics for unravelling sophisticated self-assembly processes, *Dalton Trans.*, 2006, 1473–1490.

77 G. Tircsó, M. Regueiro-Figueroa, V. Nagy, Z. Garda, T. Garai, F. K. Kálmán, D. Esteban-Gómez, É. Tóth and C. Platas-Iglesias, Approaching the Kinetic Inertness of Macrocyclic Gadolinium(III)-Based MRI Contrast Agents with Highly Rigid Open-Chain Derivatives, *Chem. – Eur. J.*, 2016, **22**, 896–901.

78 R. Ferreirós-Martínez, D. Esteban-Gómez, É. Tóth, A. de Blas, C. Platas-Iglesias and T. Rodríguez-Blas, Macrocyclic Receptor Showing Extremely High Sr(II)/Ca(II) and Pb(II)/Ca(II) Selectivities with Potential Application in Chelation Treatment of Metal Intoxication, *Inorg. Chem.*, 2011, **50**, 3772–3784.

79 C. Paul-Roth and K. N. Raymond, Amide Functional Group Contribution to the Stability of Gadolinium(III) Complexes: DTPA Derivatives, *Inorg. Chem.*, 1995, **34**, 1408–1412.

80 B. L. McNeil, S. A. Mastroianni, S. W. McNeil, S. Zeisler, J. Kumlin, S. Borjian, A. W. McDonagh, M. Cross, P. Schaffer and C. F. Ramogida, Optimized production, purification, and radiolabeling of the 203Pb/212Pb theranostic pair for nuclear medicine, *Sci. Rep.*, 2023, **13**, 10623.

81 G. L. Rothermel, L. Miao, A. L. Hill and S. C. Jackels, Macrocyclic ligands with 18-membered rings containing pyridine or furan groups: preparation, protonation, and complexation by metal ions, *Inorg. Chem.*, 1992, **31**, 4854–4859.

82 M. M. Ali, M. Woods, E. H. Suh, Z. Kovacs, G. Tircsó, P. Zhao, V. D. Kodibagkar and A. D. Sherry, Albumin-binding PARACEST agents, *JBIC, J. Biol. Inorg. Chem.*, 2007, **12**, 855–865.

83 *APEX4*, Bruker AXS Inc., Madison, Wisconsin, USA, 2021.

84 *SAINT Version 8.37A*, Bruker AXS Inc., 2015.

85 G. M. Sheldrick, *SADABS Version 2014/5*, Bruker AXS Inc.

86 G. M. Sheldrick, Crystal structure refinement with SHELXL, *Acta Crystallogr., Sect. C: Struct. Chem.*, 2015, **71**, 3–8.

87 G. M. Sheldrick, A short history of SHELX, *Acta Crystallogr., Sect. A: Found. Crystallogr.*, 2008, **64**, 112–122.

88 P. Gans, A. Sabatini and A. Vacca, Investigation of equilibria in solution. Determination of equilibrium constants with the HYPERQUAD suite of programs, *Talanta*, 1996, **43**, 1739–1753.

89 16 Gaussian, C.01 Revision, M. J. Frisch, G. W. Trucks, H. B. Schlegel, G. E. Scuseria, M. A. Robb, J. R. Cheeseman, G. Scalmani, V. Barone, G. A. Petersson, H. Nakatsuji, X. Li, M. Caricato, A. V. Marenich, J. Bloino, B. G. Janesko, R. Gomperts, B. Mennucci, H. P. Hratchian, J. V. Ortiz, A. F. Izmaylov, J. L. Sonnenberg, D. Williams-Young, F. Ding, F. Lipparini, F. Egidi, J. Goings, B. Peng, A. Petrone, T. Henderson, D. Ranasinghe, V. G. Zakrzewski, J. Gao, N. Rega, G. Zheng, W. Liang, M. Hada, M. Ehara, K. Toyota, R. Fukuda, J. Hasegawa, M. Ishida, T. Nakajima, Y. Honda, O. Kitao, H. Nakai, T. Vreven, K. Throssell, J. A. Jr., J. E. Peralta, F. Ogliaro, M. J. Bearpark, J. J. Heyd, E. N. Brothers, K. N. Kudin, V. N. Staroverov, T. A. Keith, R. Kobayashi, J. Normand, K. Raghavachari, A. P. Rendell, J. C. Burant, S. S. Iyengar, J. Tomasi, M. Cossi, J. M. Millam, M. Klene, C. Adamo, R. Cammi, J. W. Ochterski, R. L. Martin, K. Morokuma, O. Farkas, J. B. Foresman and D. J. Fox, Gaussian Inc., Wallingford CT, 2016..

90 B. Metz, H. Stoll and M. Dolg, Small-core multiconfiguration-Dirac–Hartree–Fock-adjusted pseudopotentials for post- *d* main group elements: Application to PbH and PbO, *J. Chem. Phys.*, 2000, **113**, 2563–2569.

91 K. A. Peterson, Systematically convergent basis sets with relativistic pseudopotentials. I. Correlation consistent basis sets for the post- *d* group 13–15 elements, *J. Chem. Phys.*, 2003, **119**, 11099–11112.

92 NBO Version 3.1, E. D. Glendening, A. E. Reed, J. E. Carpenter and F. Weinhold, 2003..

 